Check for updates

Received: 12 May 2023 | Revised: 30 October 2023 | Accepted: 14 November 2023

DOI: 10.1002/alz.13703

Alzheimer's & Dementia®
THE JOURNAL OF THE ALZHEIMER'S ASSOCIATION

RESEARCH ARTICLE

Silencing *Apoe* with divalent-siRNAs improves amyloid burden and activates immune response pathways in Alzheimer's disease

Chantal M. Ferguson[1] | Samuel Hildebrand[1] | Bruno M. D. C. Godinho[1] | Julianna Buchwald[1] | Dimas Echeverria[1] | Andrew Coles[1] | Anastasia Grigorenko[2] | Lorenc Vangjeli[1] | Jacquelyn Sousa[1] | Nicholas McHugh[1] | Matthew Hassler[1] | Francesco Santarelli[3] | Michael T. Heneka[3] | Evgeny Rogaev[2] | Anastasia Khvorova[1]

[1]RNA Therapeutics Institute, University of Massachusetts Medical School, Worcester, Massachusetts, USA

[2]Department of Psychiatry, University of Massachusetts Medical School, Worcester, Massachusetts, USA

[3]Luxembourg Centre for Systems Biomedicine (LCSB), Esch-sur-Alzette, Luxembourg

Correspondence
Anastasia Khvorova and Chantal M. Ferguson, RNA Therapeutics Institute, University of Massachusetts Medical School, 368 Plantation Street, Worcester, MA 01605, USA.
Email: Anastasia.khvorova@umassmed.edu and ferguson.chantal@gmail.com

Funding information
NS, Grant/Award Numbers: 104022, GM-131839, S10 OD020012, ADDF 20170101; National Research Service Award, Grant/Award Numbers: 1F30AG066373-01, T32GM107000

Abstract

INTRODUCTION: The most significant genetic risk factor for late-onset Alzheimer's disease (AD) is *APOE4*, with evidence for gain- and loss-of-function mechanisms. A clinical need remains for therapeutically relevant tools that potently modulate *APOE* expression.

METHODS: We optimized small interfering RNAs (di-siRNA, GalNAc) to potently silence brain or liver *Apoe* and evaluated the impact of each pool of *Apoe* on pathology.

RESULTS: In adult 5xFAD mice, siRNAs targeting CNS *Apoe* efficiently silenced *Apoe* expression and reduced amyloid burden without affecting systemic cholesterol, confirming that potent silencing of brain *Apoe* is sufficient to slow disease progression. Mechanistically, silencing *Apoe* reduced APOE-rich amyloid cores and activated immune system responses.

DISCUSSION: These results establish siRNA-based modulation of *Apoe* as a viable therapeutic approach, highlight immune activation as a key pathway affected by *Apoe* modulation, and provide the technology to further evaluate the impact of *APOE* silencing on neurodegeneration.

KEYWORDS
Alzheimer's Disease, Apoe, neurodegeneration, oligonucleotide therapeutics, RNAi, siRNA

1 | BACKGROUND

Alzheimer's disease (AD) is a progressive, multifactorial neurodegenerative condition for which many available medications provide only short-term alleviation of symptoms,[1,2] and the long-term impacts of newer therapies, including aducanumab and lecanemab, have yet to be determined. In late-onset AD, the apolipoprotein E gene (*APOE*) ε4 allele is the strongest genetic risk factor, and its presence is associated with an increase in AD incidence and a decrease in the age of clinical onset.[3–5] The apoE protein is mainly produced in the central nervous system (CNS) and liver. In the CNS, glial cells (and to a lesser extent, neurons) express apoE which transports lipids between cells and modulates the inflammatory response.[6,7] Liver apoE facilitates lipid uptake into peripheral tissues via low-density lipoprotein (LDL)

Chantal M. Ferguson and Samuel Hildebrand contributed equally to this study.

This is an open access article under the terms of the Creative Commons Attribution-NonCommercial-NoDerivs License, which permits use and distribution in any medium, provided the original work is properly cited, the use is non-commercial and no modifications or adaptations are made.
© 2024 The Authors. *Alzheimer's & Dementia* published by Wiley Periodicals LLC on behalf of Alzheimer's Association.

receptors.[8,9] Despite decades of compelling research into the role of *APOE* in neurodegeneration, the exact mechanism remains unclear. *APOE* is implicated in protein clearance, immune activity, and lipid homeostasis; however, a clear-cut explanation for how *APOE* impacts AD, and consensus on whether it confers a gain or loss of function phenotype, do not exist.

Genetic removal or reduction of mouse or human *APOE3* and *APOE4* in AD models reduces beta-amyloid (Aβ) plaques.[10–13] Complete loss of all mouse and human *APOE* isoforms, however, causes spontaneous atherosclerosis in mice.[14] The tissue-specific effects of *APOE* knockout are likely due to the differential roles of liver and CNS *APOE*. Previous success in genetically manipulating liver-specific or brain-specific *Apoe* in mice suggests that *Apoe* pools are independent.[15,16] However, the effects of *APOE* mRNA modulation with small interfering RNAs (siRNAs) after birth—a therapeutically-relevant paradigm—are less clear.

Reduction of brain *APOE* mRNA (≈50% of normal levels) using antisense oligonucleotides (ASO) had no significant impact on amyloid burden in adult AD mice, and neonatal treatment in models of AD was necessary to produce any significant effects.[17] Although this could suggest that embryonic *APOE* silencing is required to reduce AD phenotypes, it is also possible that residual (≈50%) *APOE* expression in the CNS or from the systemic circulation suffices to maintain pathology. Similarly, removing one copy of mouse *Apoe* only modestly improves amyloid pathology.[13] Conversely, in models of tauopathy, a 50% reduction in *APOE with* ASOs was sufficient to reduce markers of neurodegeneration.[18] Thus, ameliorating amyloid pathology might require near complete silencing of *APOE* in the adult brain.

siRNAs guide potent and sustained gene silencing in vivo via an RNA-induced silencing complex (RISC), and the chemical architecture of an siRNA determines its distribution.[19] For example, GalNAc-conjugated siRNAs selectively deliver to liver hepatocytes,[20–22] and a single injection supports 6 to 12 months of clinical efficacy.[23] We have recently described a divalent (di)-siRNA scaffold that is efficiently taken up by neurons and glial cells and supports potent, sustained, and specific target silencing throughout the CNS.[24]

Here, we engineered siRNAs targeting mouse *Apoe* and achieved silencing of liver and CNS *Apoe* in APP/PSEN1 and 5×FAD mouse models. Near-complete silencing of liver *Apoe* in APP/PSEN1 mice increased serum cholesterol with no detectable impact on brain *Apoe* or Aβ pathology. Potent reduction of CNS *Apoe*, either before or after the onset of AD pathology, decreased Aβ burden with no detectable effect on systemic cholesterol and no significant off-target effects. Like studies using genetic knockout, ASOs, and antibodies, we show that silencing *Apoe* with siRNAs reduces APOE-rich plaque cores and modulates immune system responses that may promote Aβ clearance. Compared to antibodies, siRNAs show excellent target specificity, thus, siRNAs targeting *Apoe* may have a distinct advantage over other modalities. Collectively, these results identify siRNA-mediated silencing of *APOE* as a potential therapeutic for AD in a landscape where safe and effective disease-modifying therapies are limited.

RESEARCH IN CONTEXT

1. **Systematic review**: The authors reviewed the literature using traditional (ie, PubMed) sources as well as meeting abstracts and presentations. *APOE's* role in AD has been extensively investigated and the most relevant or seminal publication addressing each point was cited.
2. **Interpretation**: We optimized therapeutic siRNAs that downregulate *Apoe* expression. Our findings show that potent downregulation of CNS APOE with siRNAs, even after the onset of cellular changes, strikingly reduces amyloid pathology in adult mice via immune activation.
3. **Future directions**: This study establishes siRNA-based silencing of brain *APOE* as a viable therapeutic approach for AD and provides directly translatable technology for therapeutic development. With these tools, it is possible to further investigate *APOE's* role in immune regulation, the temporal impact of *APOE* on disease progression, and the safety of modulating *APOE* in adult brains. We hope these results aid in developing desperately needed disease modifying therapeutics.

2 | METHODS

2.1 | siRNA sequences (Table 1)

siRNAs targeting *Apoe* (both di-siRNA and GalNAc siRNA) target a 19 base pair region of the endogenous mouse *Apoe* mRNA with the following sequence: TGGATATGGATGTTGTTGC. The targeting sequence for the non-targeting (vehicle) controls (NTC) is GCAACAACATCCATATCCA. We designed asymmetric di-siRNAs with a 20 base pair antisense and 15 base pair sense strands and GalNAc conjugated sRNAs with a 22 base pair antisense and 20 base pair sense strands. Every nucleotide is modified at the 2´hydroxyl (OH) position with either an O-methyl (m) or Flouro (modification). Phosphorothioate backbone modifications (PS, denoted as #) are included on both sense and antisense strands, at the 5´and 3´ends. The detailed sequence information is presented in Table 1 and below.

2.1.1 | Di-siRNA^{APOE}

The sense strand is CyMN3-(mA)#(mA)#(fC)(mA)(fU)(mC)(fC)(mA)(fU)(mA)(mU)(mC)(fC)#(mA)#(mA)-DIO, and the antisense strand is V(mU)#(fU)#(mG)(fG)(fA)(fU)(mA)(fU)(mG)(fG)(mA)(fU)(mG)#(fU)#(mU)#(fG)#(mU)#(mU)#(mG)#(fC).

2.1.2 | Di-siRNA^{NTC}

The sense strand is CyMN3-(mU)#(mG)#(fA)(mC)(fA)(mA)(fA)(mU)(fA)(mC)(mG)(mA)(fU)#(mU)#(mA)-DIO, and the antisense strand is

15525279, 2024, 4, Downloaded from https://alz-journals.onlinelibrary.wiley.com/doi/10.1002/alz.13703 by Cochrane Luxembourg, Wiley Online Library on [23/01/2026]. See the Terms and Conditions (https://onlinelibrary.wiley.com/terms-and-conditions) on Wiley Online Library for rules of use; OA articles are governed by the applicable Creative Commons License

TABLE 1 Detailed sequence and chemical modification patterns of siRNAs.

Name	Gene	Accession number	Sense strand	Anti-sense strand
Di-siRNA^{APOE}	Mouse ApoE	NM_009696	CyMN3-(mA)#(mA)#(fC)(mA)(fU)(mC)(fC)(mA)(fU)(mA)(mU)(mC)(fC)#(mA)#(mA)-DIO	V(mU)#(fU)#(mG)(fG)(fA)(fU)(mA)(fU)(mG)(fG)(mA)(fU)(mG)#(fU)#(mU)#(fG)#(mU)#(mU)#(mG)#(fC)
Di-siRNA^{NTC}	N/A	N/A	CyMN3-(mU)#(mG)#(fA)(mC)(fA)(mA)(fA)(mU)(fA)(mC)(mG)(mA)(fU)#(mU)#(mA)-DIO	V(mU)#(fA)#(mA)(fU)(fC)(fG)(mU)(fA)(mU)(fU)(mU)(fG)(mU)#(fC)#(mA)#(fA)#(mU)#(mC)#(mA)#(fU)
GalNAc-siRNA^{APOE}	Mouse ApoE	NM_009696	CyMN3-(mG)#(fC)#(mA)(fA)(mC)(fA)(mA)(fC)(mA)(fU)(mC)(fC)(mA)(fU)(mA)(mU)(mC)(fC)#(mA)#(mA)-GalNac	V(mU)#(fU)#(mG)(fG)(fA)(fU)(mA)(fU)(mG)(fG)(mA)(fU)(mG)(fU)(mU)(fG)(mU)(fU)(mG)(fC)#(mA)#(mG)
GalNAc-siRNA^{NTC}	N/A	N/A	CyMN3-(mA)#(fU)#(mG)(fA)(mU)(fU)(mG)(fA)(mC)(fA)(mA)(fA)(mU)(fA)(mC)(mG)(mA)(fU)#(mU)#(mA)-GalNac	V(mU)#(fA)#(mA)(fU)(fC)(fG)(mU)(fA)(mU)(fU)(mU)(fG)(mU)(fC)(mA)(fA)(mU)(fC)(mA)(fU)#(mG)#(mA)

Note: Chemical modifications are designated as follows: "#" = phosphorothioate bond, "m" = 2′-O-Methyl, "f" = 2′-Fluoro, "P" = 5′ phosphate, "V" = -5′-(*E*)-vinylphosphonate. DIO, di-siRNA; di, divalent; siRNA, small interfering RNA. Di-siRNA, divalent small interfering RNA.

V(mU)#(fA)#(mA)(fU)(fC)(fG)(mU)(fA)(mU)(fU)(mU)(fG)(mU)#(fC)#(mA)#(fA)#(mU)#(mC)#(mA)#(fU).

2.1.3 | GalNAc-siRNA^{APOE}

The sense strand is CyMN3-(mG)#(fC)#(mA)(fA)(mC)(fA)(mA)(fC)(mA)(fU)(mC)(fC)(mA)(fU)(mA)(mU)(mC)(fC)#(mA)#(mA)-GalNac, and the antisense strand is V(mU)#(fU)#(mG)(fG)(fA)(fU)(mA)(fU)(mG)(fG)(mA)(fU)(mG)(fU)(mU)(fG)(mU)(fU)(mG)(fC)#(mA)#(mG).

2.1.4 | GalNAc-siRNA^{NTC}

The sense strand is CyMN3-(mA)#(fU)#(mG)(fA)(mU)(fU)(mG)(fA)(mC)(fA)(mA)(fA)(mU)(fA)(mC)(mG)(mA)(fU)#(mU)#(mA)-GalNac, and the antisense strand is V(mU)#(fA)#(mA)(fU)(fC)(fG)(mU)(fA)(mU)(fU)(mU)(fG)(mU)(fC)(mA)(fA)(mU)(fC)(mA)(fU)#(mG)#(mA).

2.2 | Oligonucleotide synthesis

Oligonucleotides were synthesized using modified (2′-Fluoro, 2′-O-Methyl, Locked Nucleic Acid (LNA)) phosphoramidites with standard protecting groups. Phosphoarmidite solid-phase synthesis was done on a MerMade12 (BioAutomation) using modified protocols. Unconjugated oligonucleotides were synthesized on controlled pore glass (CPG) functionalized with a long-chain alkyl amine (LCAA) and unylinker terminus (ChemGenes). GalNAc-conjugated oligonucleotides were grown on custom 3′GalNAc-CPG,[25] divalent oligonucleotides (DIO) were synthesized on modified solid support,[24] and vinyl-phosphonate (VP) phosphoramidite was synthesized as described.[26] Phosphoramidites were prepared at 0.1 M in anhydrous acetonitrile (ACN), with added dry 15% dimethylformamide (DMF) in the 2′-OMe U amidite. 5-(Benzylthio)−1H-tetrazole (BTT) was used as the activator at 0.25 M. Detritylations were performed using 3% trichloroacetic acid in dichloromethane (DCM). Capping was done with non-tetrahydrofuran-containing reagents CAP A, 20% n-methylimidazole in can, and CAP B, 20% acetic anhydride (Ac_2O), and 30% 2,6-lutidine in ACN (synthesis reagents were purchased at AIC). Sulfurization was performed with 0.1 M solution of 3-[(dimethylaminomethylene)amino]−3H-1,2,4-dithiazole-5-thione (DDTT) in pyridine (ChemGenes) for 3 minutes. Phosphoramidite coupling times were 3 minutes for all amidites used.

2.3 | VP deprotection

The VP-containing oligonucleotides, still on solid support, were treated post synthesis with an anhydrous mixture of trimethylsilyl bromide/ACN/DMF/pyridine (3:9:9:1) for 1 hour at room temperature with gentle agitation. The reaction was then quenched with water and the CPG was then rinsed with ACN, DCM, and allowed to dry, before being deprotected normally as described below.

2.4 | Deprotection and purification of oligonucleotides

Divalent and conjugated oligonucleotides (DIO, GalNAc) were cleaved and deprotected with standard conditions using aqueous ammonia at 55°C for 16 hours. VP-containing oligonucleotides were cleaved and deprotected as described.[26] Briefly, CPG-containing VP-oligonucleotides were treated with a solution of 3% Diethylamine (DEA) in aqueous ammonia at 35°C for 20 hours. The solutions containing deprotected oligonucleotides were filtered to remove the CPG, and dried under vacuum in Speed-vac. The resulting pellets were re-suspended in 5% ACN in water. Purification was performed on an

15525279, 2024, 4, Downloaded from https://alz-journals.onlinelibrary.wiley.com/doi/10.1002/alz.13703 by Cochrane Luxembourg, Wiley Online Library on [23/01/2026]. See the Terms and Conditions (https://onlinelibrary.wiley.com/terms-and-conditions) on Wiley Online Library for rules of use; OA articles are governed by the applicable Creative Commons License

Agilent 1290 Infinity II HPLC system, equipped with a Source 15Q anion exchange column (GE Healthcare) using the following conditions: eluent A, 20% ACN, 20 mM sodium acetate pH 7; eluent B, 1 M sodium perchlorate in 20% ACN; gradient, 10% B 3 min to 35% B 18 min, at 60 °C. Peaks were monitored at 260 nm. Pure fractions were collected and dried in Speed-vac. Oligonucleotides were re-suspended in 5% ACN and desalted through fine Sephadex G-25 media (GE Healthcare), and lyophilized.

2.5 | Liquid chromatography-mass spectrometry (LC-MS) analysis of oligonucleotides

The identity of oligonucleotides were verified by liquid chromatography-mass spectrometry (LC-MS) analysis on an Agilent 6530 accurate mass Q-TOF using the following conditions: buffer A, 100 mM hexafluoroisopropanol (HFIP)/9 mM triethylamine (TEA) in LC-MS grade water; buffer B, 100 mM HFIP/9 mM TEA in LC-MS grade methanol; column, Agilent AdvanceBio oligonucleotides C18; gradient 0% B 1 min, 0% to 40% B 8 min, temperature, 45°C; flow rate, 0.5 mL/min. LC peaks were monitored on UV (260 nm). MS parameters: source, electrospray ionization; ion polarity, negative mode; range, 100 to 3200 m/z; scan rate, 2 spectra/second; capillary voltage, 4000; fragmentor, 180 V. Reagents were purchased from Fisher Scientific, Sigma Aldrich, and Oakwood Chemicals, and used per manufacturer's instructions, unless otherwise stated.

2.6 | Animal studies

All experimental studies involving animals were approved by the University of Massachusetts Medical School Institutional Animal Care and Use Committee (IACUC Protocols #A-2411 and #A-1744) and performed according to the guidelines and regulations therein described. APP/PSEN1 (MMRRC 34832-JAX) mice were bred in house and obtained from Jackson Lab. 5xFAD mice (MMRRC Stock No: 34840-JAX) were obtained from Jackson Lab (experiments were performed on hemizygote APP/PSEN1 and 5xFAD mice). Initial aged APP/PSEN1 mouse colonies were a gift from Dr. Arya Biragyn from the National Institute on Aging.

To determine ideal sample size, we performed a power calculation using published data in transgenic mice, and preliminary data evaluating efficacy of the siRNAs used in this study. In published data, the genetic removal of *Apoe* (100%) in transgenic AD models resulted in greater than 90% pathologic improvement, and ≈50% *Apoe* silencing with ASOs results in ≈10% reduction in pathology. As shown in Alterman et al.,[24] the *Apoe*-targeting siRNAs silence > 95% of APOE in the brain. Thus, we based the calculation off a predicted mean reduction in amyloid burden of 50% after treatment with siRNAs targeting *Apoe*, and a standard deviation of 25%. To achieve 95% power with an alpha level of 0.01, 9 animals would be required per group. The complete power calculation is included in Table S1.

2.7 | Stereotactic ICV injections

A total of 237 μg di-siRNA in 10 μL was administered into the lateral ventricles of mice as previously described.[24] The dose was split between each ventricle, for 118 μg di-siRNA in 5 μLs per lateral ventricle. Briefly, mice were anesthetized using avertin and prepared using standard aseptic technique. Stereotaxic devices were using to hold injection needles and identify injection location. After the identification of the bregma, the needle was placed 1 mm laterally, 0.2 mm posterior, and 2.5 mm caudally. Injection was performed at 500 nL/minute. Mice were then monitored until fully sternal.

2.8 | Sub-cutaneous injections

GalNAc-conjugated siRNAs were injected subcutaneously (SC) into mice. Each animal received a 10 mg/kg dose in 200 μL volume. For anti-siRNAs, mice received 1 mg/kg SC.

2.9 | Tissue collection

mRNA quantification was performed as previously described.[24] Briefly, tissue punches were stored in RNAlater (Invitrogen #AM7020) and homogenized in QuantiGene 2.0 homogenizing buffer (Invitrogen, QG0517) with proteinase K (Invitrogen, 25530-049). mRNA was detected according to the QuantiGene 2.0 protocol using the following probe sets: mouse HPRT (SB-15463), mouse PPIB (SB-10002), mouse *apoE* (SB-13611).

2.10 | Protein quantification

For analysis of APOE protein expression in mouse brain samples, WES by ProteinSimple was used as previously described.[24,27] Briefly, tissue punches were collected as above and flash-frozen, and placed at −80°C. After the addition of radioimmunopreciptation assay (RIPA) buffer with protease inhibitors, samples were homogenized and stored at −80°C. Protein amount was determined using Bradford Assay. Samples were diluted in 0.1× sample buffer (ProteinSimple) to ≈0.2 to 0.4 μg/μL. Anti-APOE antibody (Abcam, 183597) was diluted 1:200 in antibody diluent (ProteinSimple) and loading control, anti-Vinculin (Invitrogen, 700062), was diluted 1:1000 in antibody diluent. The assay was performed as described by ProteinSimple protocol using the 16 to 230 kDa plate (SM-W004). The separation electrophoresis and immunodetection are performed automatically in the capillary system using the default system settings. Once loaded, the separation electrophoresis was performed automatically. Results were analyzed using the Compass for Protein Simple software.

Amyloid precursor protein (APP), carboxy-terminal fragments (CTFs), and Aβ42 protein were evaluated using traditional western blots. In brief, snap-frozen hippocampal and cortical brain samples

15525279, 2024, 4, Downloaded from https://alz-journals.onlinelibrary.wiley.com/doi/10.1002/alz.13703 by Cochrane Luxembourg, Wiley Online Library on [23/01/2026]. See the Terms and Conditions (https://onlinelibrary.wiley.com/terms-and-conditions) on Wiley Online Library for rules of use; OA articles are governed by the applicable Creative Commons License

were extracted in phosphate-buffered saline (PBS), 1 mM EDTA, 1 mM EGTA, and 3 μL/mL protease inhibitor mix (Sigma, Munich, Germany) as previously described.[28] Homogenates were extracted in RIPA buffer (25 mM Tris-HCl, pH 7.5, 150 mM NaCl, 1% NP40, 0.5% NaDOC, 0.1% sodium dodecyl sulfate [SDS]), centrifuged at 100,000 × g for 30 minutes and the pellet containing insoluble Aβ was solubilized in 2% SDS, 25 mM Tris-HCl, pH 7.5. In addition, the SDS-insoluble pellet was extracted with 70% formic acid in water. Formic acid was removed using a speed vac (Eppendorf, Hamburg, Germany) and the resulting pellet was solubilized in 200 mM Tris-HCl, pH 7.5. Samples were separated by 4% to 12% NuPAGE (Invitrogen, Karlsruhe, Germany) using MES or MOPS buffer and transferred to nitrocellulose membranes. APP and Aβ were detected using antibody 6E10 (Covance, Münster, Germany) and the c-terminal APP antibody 140 (CT15). α-tubulin served as housekeeping control. Immunoreactivity was detected by enhanced chemiluminescence reaction (Millipore, Darmstadt, Germany) or near-infrared detection (Odyssey, LI-COR). Chemiluminescence intensities were analyzed using the ChemiDoc XRS documentation system (Bio-Rad, Munich, Germany).

2.11 | Cholesterol

Serum cholesterol was measured using the Abcam LDL and high-density lipoprotein (HDL) cholesterol quantification kit (ab65390). LDL and HDL were separated using the included precipitation buffer that uses a water-soluble non-ionic polymer to precipitate the fractions.[29] The assay uses cholesterol esterase to hydrolyze cholesteryl ester into free cholesterol. Next, cholesterol oxidase acts on free cholesterol to produce a color at 570 nm that is proportional to the amount of cholesterol in the sample. Briefly, serum was collected prior to euthanasia. A 2× buffer was added to 50 μL of serum and incubated at room temperature for 10 minutes. Samples were spun for 10 minutes at 2000 rpm and the supernatant (LDL fraction) was placed in a separate tube. The pellet (HDL fraction) was resuspended in 200 μL PBS. The samples were diluted, and cholesterol levels were analyzed according to the package instructions.

2.12 | Histology and analysis

See Table S2 for key resources used.

For evaluation of amyloid plaque burden, four 40-μm formalin-fixed brain slices per animal were stained in a free-floating format with either X-34 dye (Sigma-Aldrich, #SML1954), APP6E10 (BioLegend, #803001), or Aβ42 (Cell Signaling, D9A3A). For X-34 staining, formalin-fixed brain slices were washed in PBS for 5 minutes, incubated in 100 μM ×-34 (dissolved in 40% EtOH) for 10 minutes, rinsed 5× in water, incubated in 0.2% NaOH in 80% EtOH for 2 minutes, then washed in distilled water for 10 minutes, and mounted for imaging. Images were performed with a 20× objective on a Leica inverted microscope. Number and size (area, volume) were quantified using ImageJ thresholding and 3D object counter and normalized to controls. For immunohistochemistry (IHC), three 40-μm slices were placed in 70% formic acid for 15 minutes, washed three times in PBS, placed in 1% H_2O_2 for 30 minutes, washed three times in PBS, blocked and permeabilized in 10% blocking serum and 0.5% Triton-X. Samples were placed in biotin-°labeled APP 6E10 (BioLegend #803007) at 4°C overnight and developed using ABC (VectorLabs #PK-6200) DAB peroxidase system (VectorLabs #SK-4100). Samples were allowed to dry and dehydrated in ethanol, cleared with xylenes and cover slipped. Images were acquired with a 5× objective using tiling. Analysis was performed using ImageJ. Briefly, images were converted to 8-bit images. Thresholding was applied to measure the number and size of amyloid plaques. Amyloid burden was reported as percent of the total area measured. Values across at least three slices per animal were averaged and compared to controls.

For immunofluorescence, slices were treated with 70% formic acid for 15 minutes, incubated in blocking buffer (PBS with 1% bovine serum albumin [BSA] and 0.3% Triton X-100) for 1 hour at room temperature, incubated with primary antibodies overnight at rotating 4°C (APP6E10: 1:1000, Aβ42: 1:200, APOE: 1:500, GFAP 1:500), washed with PBS, incubated with Alexa-Fluor-labeled secondary antibodies diluted 1:500 in blocking buffer for 2 hours at room temperature, washed with PBS, and mounted with ProLong Diamond. Imaging was performed on a Leica inverted microscope.

2.13 | Microglial clustering

Samples were processed for immunofluorescence as described above with IBA1 primary antibody (ab178846, 1:500) and Alexa-Fluor-labeled secondary antibodies diluted 1:500. The Z-stack of images (at 1 μm interval for 40 μm slice) for five random regions of interest per animal were acquired from the cortex using a Leica inverted microscope at 63× resolution. Manually going through the Z-stack the number of microglia cells where quantified using a cell counter and assigned to one of the two categories: free-standing and clustered microglia. The clustered microglia (or plaque-associated) were defined as being within proximity, including the cell body or processes overlapping with, the amyloid plaque. The number of free and clustered (plaque-associated) microglia per field of view was quantified using the cell counter in ImageJ. The numbers were averaged for five sections per animal, and the data presented show the resulting calculations for the n-4,5 animals.

2.14 | Aβ enzyme-linked immunosorbent assays

For APP/PSEN1 mice, Aβ42 (Thermo Fisher, #KHB3544) and Aβ40 (Thermo Fisher, #KHB3481) were measured using enzyme-linked immunosorbent assays (ELISAs). For 5×FAD mice, Aβ42, Aβ40, and Aβ38 were quantified using multiplex Meso Scale Discovery (MSD) plates (MSD, #K15200E). Brain homogenates were solubilized in RIPA buffer with protease inhibitors and spun down for 20 minutes. The RIPA fraction was transferred to a new tube. The pellet was

15525279, 2024, 4, Downloaded from https://alz-journals.onlinelibrary.wiley.com/doi/10.1002/alz.13703 by Cochrane Luxembourg, Wiley Online Library on [23/01/2026]. See the Terms and Conditions (https://onlinelibrary.wiley.com/terms-and-conditions) on Wiley Online Library for rules of use; OA articles are governed by the applicable Creative Commons License

resuspended in 70% formic acid and incubated rotating for 2 hours. Samples were then spun down and the supernatant transferred to a new tube and used for ELISA assays. ELISAs and MSD assays were performed and analyzed according to the manufacturer's instructions.

Please see Table S2 for key resources used.

2.15 | RNA sequencing and data analysis

2.15.1 | Library preparation

RNA from brain punches was purified using the NEB RNA purification kit (NEB, #T2010S). RNA libraries were prepared using a TruSeq kit (Illumina, #20020595). Samples were run on HiSeq Flow 4000 for NextSeq 550 single end with read lengths of 100 and 72, respectively. Reads were then mapped to a custom mm10 genome containing human APP for the APP/PSEN1 mice, a custom genome containing human APP and PSEN1 for the 5XFAD mice, and a custom genome of mm10 containing human APP, using STAR v2.7.6a[30] and transcript expression was calculated with RSEM v1.3.3.[31] Genes with an estimated count of less than 5 in at least half the samples were removed from further analysis.

2.15.2 | Differential expression

Differential expression was calculated with DESeq2 v1.22.2 using an alpha of 0.05 and apeglm log2 fold change shrinkage.[32,33] The presence of siRNA seed complementarity (7-mer complementary to siRNA guide strand positions 2 to 8) in all genes with annotated 3′-UTRs in Ensembl. GRMCm38.p6 annotations were determined with a custom Python script. siRNA seed enrichment in downregulated versus unchanged and upregulated transcripts was calculated using a Fisher Exact Test. Data were plotted using Matplotlib.

2.15.3 | Gene set enrichment analysis

Gene set enrichment analysis was conducted using the fgsea R package[34] and plotted using the viseago R package,[35] with custom settings for heatmap color to indicate if a gene set is upregulated or downregulated.

2.15.4 | Weighted gene co-expression network analysis

Data for weighted gene co-expression network analysis (WGCNA)[36] were first filtered to remove genes with 10 or fewer reads in any sample, batch effect-corrected for sex using the ComBat-Seq R package,[37] and transformed using the vst function in DESeq2. WGCNA with additional k-means clustering was conducted using the CoExpNets R package[38] with default settings. Gene ontology of modules was performed with gprofiler2.[39]

2.15.5 | Disease-associated microglia subtype analysis

Marker genes for disease-associated microglia (DAM) were taken from previously published single-cell RNA sequencing data.[40–43] A custom GMT file was created using these marker genes and GSEA was performed with this GMT file with GSEAPY, using 1000 permutations. Pearson correlation of *Apoe* to each gene in the set of marker genes for DAM was calculated using corr.test in R and DESeq2 variance stabilized transformed counts

2.15.6 | Transcription factor enrichment analysis

Transcription factor enrichment analysis of upregulated genes was performed using the MAGIC 1.1 python package, using the "1 kb_gene" matrix.[44] The transcription factor enrichment score was calculated as the ratio of the observed versus expected number of genes controlled by a transcription factor. The transcription factor enrichment score was calculated for genes upregulated in the 5XFAD 2-month and displayed as a bar graph plot.[45,46]

2.16 | Statistics

Each n represents an independent biological sample. All graphs show means ± S.D. All statistics were performed using Prism GraphPad v.8, using either two-tailed, unpaired *t*-tests or one-way analysis of variance (ANOVA) with Dunnett correction. Box plots show the following statistics: center line, median; top of the box, 75% quartile; bottom of the box, 25% quartile; whiskers, minimum and maximum.

3 | RESULTS

3.1 | CNS and systemic *Apoe* are spatially and functionally distinct in APP/PSEN1 mice

Tissue-specific *Apoe* knockouts have revealed that CNS and systemic *Apoe* are independently maintained in mice.[15,16] To determine if siRNA silencing of *Apoe* in the CNS impacts liver *Apoe* and vice versa, we engineered chemically modified siRNAs targeting mouse *Apoe* in either a liver-active ($GalNAc^{APOE}$) or CNS-active ($di\text{-}siRNA^{APOE}$) chemical configuration (*Apoe* targeting sequence: TGGATATGGATGTTGTTGC) (Table 1). The targeting sequences were chosen based on previously published screen.[47] Briefly, a panel of siRNAs targeting mouse *Apoe* were screened in primary mouse astrocytes. Hits were chosen based on maximum silencing and evaluated with a seven-point dose-response study to determine IC50 values. ApoE 1134 was chosen as a lead

15525279, 2024, 4, Downloaded from https://alz-journals.onlinelibrary.wiley.com/doi/10.1002/alz.13703 by Cochrane Luxembourg, Wiley Online Library on [23/01/2026]. See the Terms and Conditions (https://onlinelibrary.wiley.com/terms-and-conditions) on Wiley Online Library for rules of use; OA articles are governed by the applicable Creative Commons License

compound based on maximum silencing and IC50 value in cells. The compound was tested in wild type mice and showed good efficacy (>95% silencing, $p < 0.001$) 2 months post injection.[24]

To silence brain *Apoe*, 2-month-old APP/PSEN1 mice (JAX#34832)[48–50] were injected intracerebroventricularly (ICV) with a total of 237 μg (118.5 μg into each lateral ventricle) of di-siRNA^{APOE} and compared to a non-targeting control (NTC) group (di-siRNA^{NTC}). To silence liver *Apoe*, a second group was injected subcutaneously (SC) with 10 mg/kg GalNAc^{APOE} and compared to a non-targeting control (NTC) group (GalNAc^{NTC}). Two months post-injection, when animals were 4 months old, we measured *Apoe* mRNA and protein in the brain and the liver, and serum cholesterol levels (Figure 1A,B, Figure S1a,b). In di-siRNA^{APOE}-treated mice, we observed >90% *Apoe* mRNA and >95% protein silencing ($p < 0.0001$) in the brain and ≈50% silencing in the liver ($p < 0.0001$) compared controls (Figure 1C,D). In GalNAc^{APOE}-treated mice, we observed >99% *Apoe* mRNA and protein silencing in the liver ($p < 0.0001$) and no silencing in the brain (Figure S1c,d, Figure S2 for raw western blots).

Despite the partial reduction of liver *Apoe* in di-siRNA^{APOE} -treated mice, serum cholesterol levels remained normal (Figure 1E). In contrast, the near-complete silencing of liver *Apoe* in GalNAc^{APOE}-treated mice resulted in significantly increased LDL-cholesterol levels compared to controls (≈300%, $p < 0.001$) (Figure S1e). While we did not measure CNS cholesterol levels directly in APP/PSEN1 animals, we previously observed no significant impact of the CNS and systemic *Apoe* silencing on brain cholesterol levels in wild-type mice and only complete systemic silencing of hepatic *Apoe*-impacted circulating cholesterol levels (Ferguson et al., in submission). We observed no liver toxicity in either treatment groups compared to their respective controls using standard liver function tests (Table S3). These data confirm the efficacy of the siRNAs in the CNS and the liver. In addition, these data show, at least in the short term, that APOE protein does not readily traffic between the CNS and the systemic circulation to rescue expression after siRNA-mediated silencing, and that CNS *Apoe* does not significantly regulate systemic cholesterol levels. The ability to silence CNS *Apoe* without affecting *Apoe*'s role in regulating systemic cholesterol levels allows for the exploration of siRNA-mediated silencing of CNS *APOE* in AD.

3.2 | CNS silencing of *Apoe* reduces amyloid pathology in APP/PSEN1 model

To evaluate the effects of *Apoe* silencing on AD pathology in APP/PSEN1 mice, we measured the number and size of amyloid plaques at 2 months post-injection (4 months old). Toxic amyloid fragments (Aβ40, Aβ42) aggregate into plaques that are visible throughout the brain on postmortem histology. Amyloid plaques were detected by IHC for amyloid (APP6E10) or by X-34 staining (which is sensitive for β-pleated amyloid).[51] Amyloid plaque burden was calculated as the percentage of area positive for amyloid plaques (see Methods for details). Consistent with prior reports,[52] we observed differences in the degree of pathology between female and male mice, and thus performed sex-separated analysis; however, the relative reduction in pathology after di-siRNA^{APOE} treatment was similar between sexes (Figure 1F–M). Compared to controls, silencing *Apoe* with di-siRNA^{APOE} reduced APP6E10 positive plaque burden (female: 86%, $p < 0.0001$; male: 70%, $p = 0.0158$) (Figure 1F,H) and X-34 positive amyloid plaque burden throughout the brain in both female and male mice (female: 78%, $p < 0.0001$; male: 79%, $p = 0.0029$) (Figure 1G,K).

In addition to visible aggregated plaques, Aβ exists as fragments of toxic Aβ42 and, to a lesser extent, Aβ40 and Aβ38.[53] The role of amyloid plaques versus amyloid fragments in disease progression is not clear.[54,55] We used ELISA to measure Aβ42 or Aβ40 levels in soluble and insoluble fractions of cortical lysates. Consistent with staining studies, silencing *Apoe* resulted in reduced levels of insoluble Aβ40 (female: 56%, $p = 0.011$; male: 40%, $p = 0.0738$) (Figure 1I) and Aβ42 (female: 84%, $p < 0.0001$; male: 80%, $p = 0.0529$) (Figure 1J). Soluble Aβ42 and Aβ40 levels were similar between treatment groups (Figure 1L,M). The degree of amyloid burden differed between female and male mice, but silencing *Apoe* reduced amyloid burden pathology similarly in both sexes. Importantly, near-complete silencing of liver *Apoe* had no effect on amyloid burden or insoluble Aβ42 levels but did modestly increase soluble Aβ42 (Figure S1e–i), highlighting the importance of maintaining systemic *Apoe* expression. Collectively, our results show that near-complete silencing of CNS *Apoe* before the onset of amyloid pathology significantly reduces amyloid burden in adult APP/PSEN1 mice without affecting systemic cholesterol homeostasis.

3.3 | Silencing *Apoe* after onset of pathological changes reduces amyloid pathology in 5xFAD mice

To study the effects of silencing *Apoe* at the stage of early amyloid deposition and after the onset of underlying biological changes, we turned to the 5xFAD mouse model, which expresses humanized *APP* harboring 3 mutant alleles—Swedish (K670N, M671L), Florida (I716V), and London (V717I) alleles—and human *PSEN1* harboring two mutations (M146L and L286V). The 5xFAD mice show amyloid deposition, astrocyte activation, and neuronal cell death beginning between 6 and 8 weeks of age.[56] We injected (ICV) 9-week-old 5xFAD mice with 237 μg of di-siRNA^{APOE} or di-siRNA^{NTC} (control) and measured brain *Apoe* expression, amyloid burden, and transcriptome changes at 2 weeks and 2 months post-injection (11 and 17 weeks old, respectively) (Figure 2A,B). To account for possible variations in phenotypes between sexes, we performed a sex-separated analysis of AD phenotypes including amyloid burden and behavior; however, as siRNA silencing is not sex-dependent, we analyzed male and female mice together.

Di-siRNA^{APOE} potently silenced *Apoe* mRNA in all regions of the brain (Figure 2C) (>95%, $p < 0.0001$) at both time points. At these early time points, 5xFAD mice do not exhibit significant AD-related cognitive deficits.[56] However, treatment with di-siRNAs and subsequent silencing of *Apoe* did not result in cognitive impairment during the open field, novel object recognition (NOR), or y-maze spontaneous alternation tests at 2 months post-injection (Figure S3). While we were unable

15525279, 2024, 4, Downloaded from https://alz-journals.onlinelibrary.wiley.com/doi/10.1002/alz.13703 by Cochrane Luxembourg, Wiley Online Library on [23/01/2026]. See the Terms and Conditions (https://onlinelibrary.wiley.com/terms-and-conditions) on Wiley Online Library for rules of use; OA articles are governed by the applicable Creative Commons License

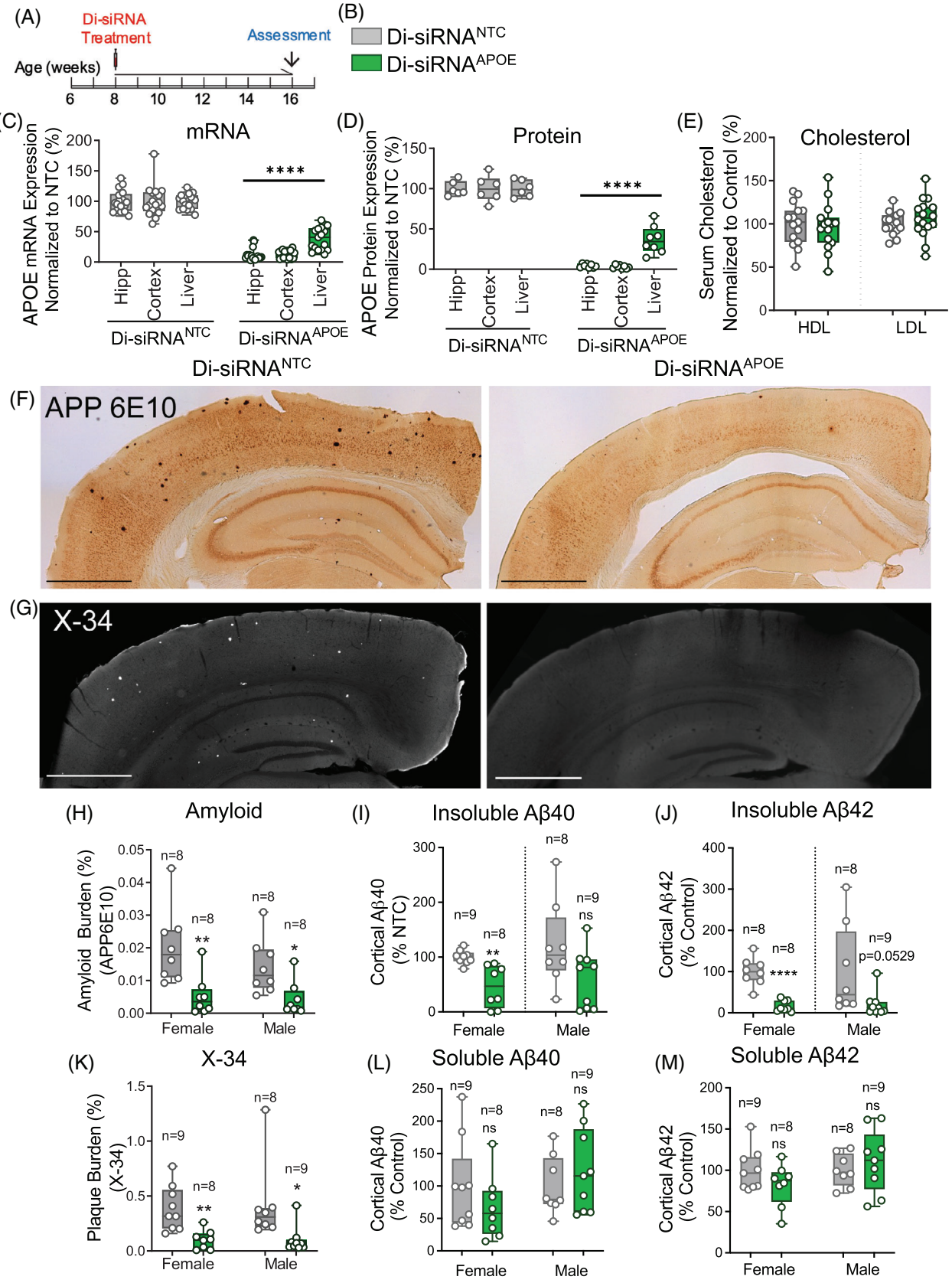

FIGURE 1 Silencing brain *Apoe* reduces AD neuropathology in APP/PSEN1 mice with no effect on serum cholesterol. (A,B) Experimental timeline. Di-siRNA dose is 237 μg. Di-siRNA^{NTC} shown in grey, and di-siRNA^{APOE} shown in green. (C,D) *Apoe* mRNA (C), and APOE protein (D) expression in the hippocampus, cortex, and liver 2 months post administration of di-siRNA^{NTC} or di-siRNA^{APOE}. (E) Serum HDL and LDL cholesterol in treated and control mice ($n = 8$ to 9 per group). (F) APP6E10 plaques in the cortex 2 months post-injection in treated mice (left) and

15525279, 2024, 4, Downloaded from https://alz-journals.onlinelibrary.wiley.com/doi/10.1002/alz.13703 by Cochrane Luxembourg, Wiley Online Library on [23/01/2026]. See the Terms and Conditions (https://onlinelibrary.wiley.com/terms-and-conditions) on Wiley Online Library for rules of use; OA articles are governed by the applicable Creative Commons License

to determine the impact on AD-related cognitive changes from these experiments, these results suggest that silencing CNS *Apoe* with siRNAs is well-tolerated in adult mice. Further studies are needed in older mice to evaluate the impact of silencing *Apoe* on the cognitive effects of AD.

At 2 weeks post-injection, treated and control animals showed early signs of amyloid pathology, with the most extensive plaque deposition being in the posterior hippocampus and entorhinal cortex and the most antibody reactivity being associated with intraneuronal APP (Figure S4a,c). There were no significant differences between groups at this time point.

At 2 months post-injection, compared to controls, we observed significantly less amyloid burden in the brains of di-siRNA^{APOE}-treated mice (Figure 2D,F,H) (Table S4). In di-siRNA^{APOE}-treated male but not female mice, amyloid plaques in the hippocampus and cortex were smaller than those in control mice ($p = 0.0206$ and $p = 0.0278$, respectively) (Figure 3A). Differences in plaque size were not observed in other regions of the brain where fewer plaques were detected. The number of amyloid plaques was significantly reduced in all brain regions in female mice (hippocampus: $p = 0.0012$; cortex: $p = 0.0003$; thalamus: $p = 0.0001$), and male mice (hippocampus: $p = 0.0020$; cortex: $p = 0041$; thalamus: $p = 0.0010$) (Figure 3B, Table S4).

The APP6E10 antibody used to measure amyloid burden detects Aβ fragments (Aβ38, 40, 42) as well as the normally processed 100-kDa APP product (Figure 2B).[57] Indeed, IHC using APP6E10 strongly stained extracellular plaques (black arrow) and diffuse intraneuronal APP in cortical and hippocampal neurons (black asterisk) (Figure 2F). To differentiate between general amyloid burden measured by APP6E10 and Aβ42-specific plaque load, we performed immunofluorescence with an Aβ42-specific antibody (Cell Signaling; D9A3A). *Apoe* silencing led to a lower Aβ42 plaque burden (Figure 2E,G,I), reduced the burden of insoluble Aβ42 measured using Multiplex ELISA MSD assays (MSD K15200E), the more toxic and aggregate-prone fragment (Figure 2J,K), and led to fewer amyloid plaques throughout the brain (Figure 3C). Interestingly, plaque size was unaffected by *Apoe* silencing (Figure 3D, Table S5) and *Apoe* silencing had no effect on soluble Aβ42 or Aβ40 levels (Figure 3E).

3.4 | Silencing *Apoe* reduces amyloid carboxyl-terminal fragments in 5xFAD mice

In AD patients, toxic amyloid plaques accumulate when the production of amyloid protein fragments is not balanced by clearance.[58] APP processing on the cell membrane produces α-CTFs by a non-amyloidogenic pathway, and β-CTFs via an amyloidogenic pathway.[58] In healthy brains, amyloid fragments are cleared by amyloid degrading enzymes (ADEs), including neprilysin, insulin-degrading enzyme (IDE), and matrix metalloproteinases.[59,60] To determine how silencing *Apoe* helps improve amyloid pathology, we measured α- and β-CTFs in hippocampal and cortical brain samples from 5xFAD mice.[61] In control animals, α- and β-CTF levels increased between time points, consistent with worsening pathology as animals age (Figure 4A–D, Figure S5a–d). Interestingly, after 2 weeks of silencing CNS *Apoe*, there was an increase in cortical CTFs and Aβ42 compared to controls. However, after 2 months of silencing CNS *Apoe*, we observed a marked reduction of cortical and hippocampal APP and Aβ42 protein (Figure 4A–D, Figure S5a–d), and a surprising reduction of both α- and β-CTFs in the cortex. Silencing *Apoe* did not significantly affect mRNA levels of APP, presenilin (PSEN1/PSEN2), or the APP-cleaving enzyme BACE1 (Figure 4E). These results suggest that long-term silencing of *Apoe* may decrease APP protein stability and may reduce the production of amyloid fragments via both amyloidogenic and non-amyloidogenic pathways, without altering the expression of APP mRNA or its processing machinery.

3.5 | Silencing *Apoe* with siRNAs reduces APOE-rich plaque cores in 5xFAD mice

Previous studies have observed that APOE is enriched in the core of amyloid plaques, suggesting that APOE serves as a scaffold for the aggregation of amyloid fragments into non-degradable plaques. The loss of the APOE core may allow for phagocytic clearance of plaques by microglia and turnover of toxic amyloid fragments.[17,45,62–67] To build upon these studies, we evaluated the presence of APOE in plaques using immunofluorescence. In controls, we observed APOE-rich (red) amyloid plaque (green) cores in 5xFAD mice (Figure 4F). Silencing *Apoe* with siRNAs reduced both amyloid plaque burden and APOE signal in plaque cores (Figure 4g). We observed residual APOE staining in occasional amyloid plaques that likely represents APOE cores that formed prior to treatment (Figure 4G, arrow). Others have previously shown that silencing *Apoe* destroys the core, allowing for phagocytic clearance of plaques by microglia and the turnover of toxic amyloid fragments.[45,66–68] We build upon these studies by showing that siRNA-mediated silencing of *Apoe* similarly reduces the APOE-rich core and subsequently, amyloid plaque burden in 5xFAD.

We next used immunofluorescence to probe the effect of removing APOE-rich cores on microglial clustering. In a subset of animals ($n = 4$ per group), five random regions of interest per animal were

controls (right). (G) X-34-positive plaques in cortex 2 months post-treatment in treated mice (left) and controls (right). (H–I) Sex-stratified quantification of APP6E10-positive cortex plaques (H), and insoluble Aβ40 fibrils (I) and insoluble Aβ 42 fibrils (J) in cortex samples. (K–M) Sex-stratified quantification of X-34-positive plaques in the cortex (K), soluble Aβ40 fibrils (L) and soluble Aβ42 fibrils (M) in cortex samples. mRNA evaluated using QuantiGene. APOE protein quantified with WES ProteinSimple; statistical analysis was one-way ANOVA or *t*-test using GraphPad Prism. Error bars are SD. Middle bars are median. Aβ, amyloid beta; AD, Alzheimer's disease; di-siRNA, divalent small interfering RNA; HDL, high-density lipoprotein; LDL, low-density lipoprotein. $^{*}p < 0.05$, $^{**}p < 0.01$, $^{***}p < 0.002$, $^{****}p < 0.0001$.

15525279, 2024, 4, Downloaded from https://alz-journals.onlinelibrary.wiley.com/doi/10.1002/alz.13703 by Cochrane Luxembourg, Wiley Online Library on [23/01/2026]. See the Terms and Conditions (https://onlinelibrary.wiley.com/terms-and-conditions) on Wiley Online Library for rules of use; OA articles are governed by the applicable Creative Commons License

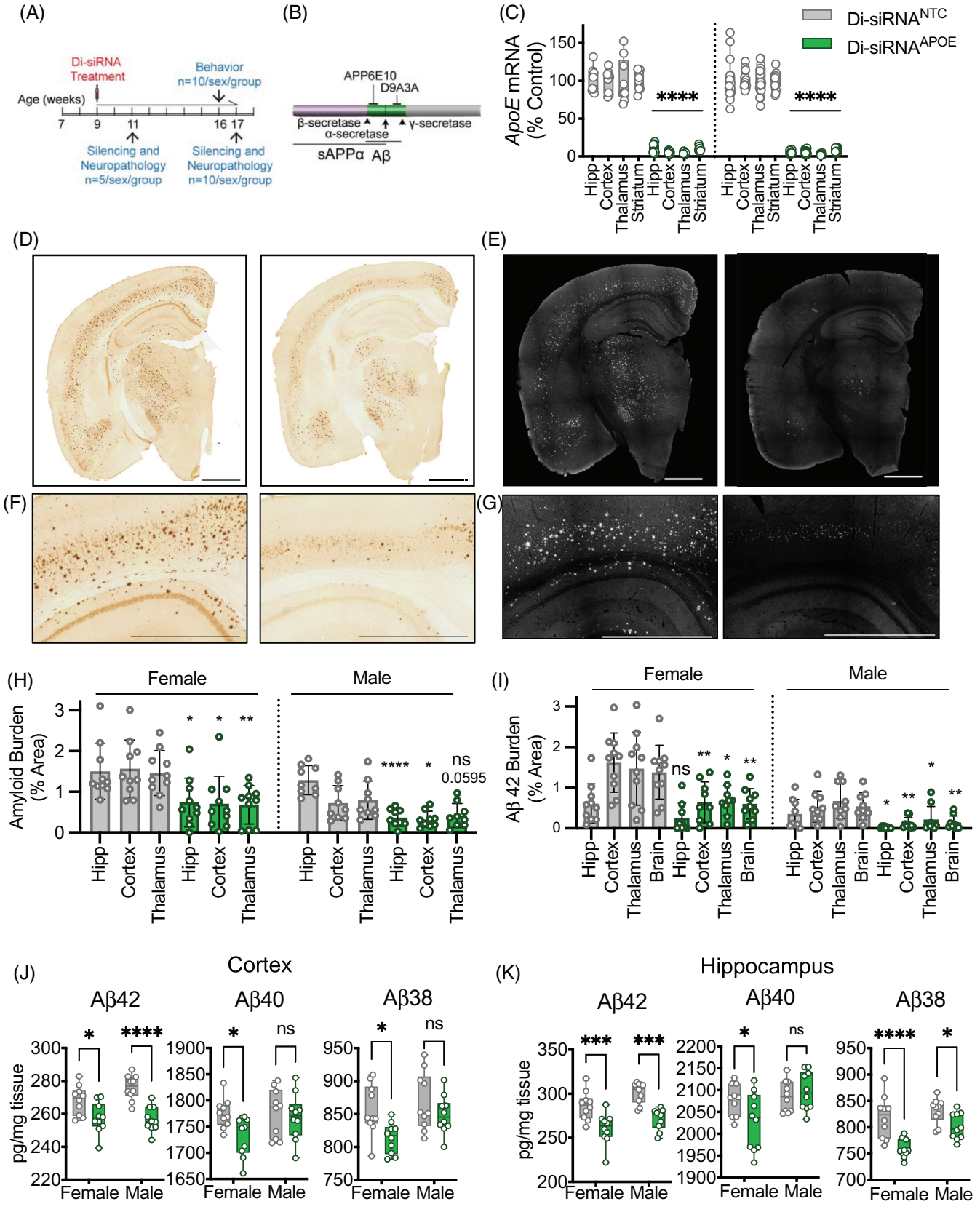

FIGURE 2 Silencing *Apoe* after the onset of pathologic changes improves amyloid burden in 5xFAD mice. (A) Experimental design. (B) Schematic showing antibody binding sites for APP6E10 and Aβ42-specific antibody (D9A3A). APP6E10 will react with Aβ and soluble APPα (sAPPα). (C) mRNA expression throughout the brain 2 weeks and 2 months post administration of di-siRNA^{APOE}. Controls (di-siRNA^{NTC}) are shown in grey and treated (di-siRNA^{APOE}) are shown in green. (D) Amyloid deposition using APP6E10 in controls (left) and treated (right) animals. Scale bar:

15525279, 2024, 4, Downloaded from https://alz-journals.onlinelibrary.wiley.com/doi/10.1002/alz.13703 by Cochrane Luxembourg, Wiley Online Library on [23/01/2026]. See the Terms and Conditions (https://onlinelibrary.wiley.com/terms-and-conditions) on Wiley Online Library for rules of use; OA articles are governed by the applicable Creative Commons License

acquired from the cortex and the number of free and clustered (plaque-associated) microglia per field of view was quantified using ImageJ (see methods). In treated and control mice, we observed IBA1-positive microglial clustering around plaques (Figure 5A–B). siRNA silencing of *Apoe* resulted in an increase in free microglia and a significant reduction of microglia clustered around plaques (Figure 5C). Although the dense clustering of microglia around plaques and the complexity of the tissue samples made it difficult to quantify ramification and branch formation, silencing *Apoe* qualitatively increased branching, suggesting that *Apoe* silencing may increase ramification. Further investigation of microglial behavioral and morphologic changes in response to *Apoe* silencing and amyloid reduction is necessary.

3.6 | *Apoe* silencing activates innate immune responses

In the early stages of AD, amyloid-degrading enzymes released by microglia cannot keep pace with the production and aggregation of toxic amyloid fragments.[69] To probe the potential impact of *Apoe* silencing on immune-driven clearance, we evaluated gene expression in both APP/PSEN1 (cortex, 2 months post-injection, $n = 8–10$/group) and 5×FAD mouse models (cortex, 2 weeks, $n = 9–10$/group; and 2 months post-injection, $n = 20$/group). Each treated group was compared to its corresponding age-matched non-targeting control group and differentially expressed genes were identified using a false discovery rate (FDR) of ≤0.05 and a log2 fold change of 0.5 (detailed further in Methods). Because the di-siRNA structure itself does not significantly alter gene expression or stimulate an inflammatory response, any changes observed here are likely a direct or downstream result of silencing *Apoe*.[24]

Apoe was the most significantly downregulated gene in 5xFAD mice at 2 weeks (log2 fold-change −3.28, $p = 7.28e^{-62}$) and 2 months (log2 fold-change −3.76, $p = 6.63e^{-165}$) post-injection, and in APP/PSEN1 mice at 2 months post-injection (−2.85, $p = 2.43e^{-18}$) (Figure 5D–F). Only two to four genes with complementarity to the di-siRNA seed sequence were marginally down-regulated, perhaps related to off-target siRNA activity. The high specificity of di-siRNAs observed here is consistent with previous reports of di-siRNAs in the CNS.[24] Thus, off-target events are unlikely to contribute to transcriptome changes.

Although we did not observe phenotypic changes in 5×FAD mice at 2 weeks post-injection, silencing *Apoe* resulted in detectable transcriptomic changes, suggesting initiation of underlying biological processes that may affect disease progression (Figure 5D). Transcriptome changes were more profound in both models after 2 months (Figure 5D–F), consistent with the significant reduction in amyloid burden. In both mouse models, the transcriptome effects of *Apoe* silencing were skewed towards gene activation (Figure 5D–F). In 5xFAD mice, 64 genes were upregulated at 2 weeks and 160 genes were upregulated at 2 months post-injection (log2 fold change cutoff of 0.5 and adjusted *p*-value cutoff of 0.05). Conversely, only 12 and 14 genes were downregulated at 2 weeks and 2 months post-treatment, respectively. Two weeks post-injection in 5xFAD mice, AD-associated genes, *Trem2*, *Slamf9*, *Tmem119*, and *Cst7* were upregulated. *Tmem119* remained slightly upregulated at 2 months, but fell just below the set threshold, while there were no significant expression differences in the other genes (Tables S6 and S7, File S1). In APP/PSEN1 mice, silencing *Apoe* resulted in significant upregulation of 21 genes and downregulation of just one.

Gene set enrichment analysis (GSEA) showed a consistent increase in innate immune processes following *Apoe* silencing, with genes involved in type 1 interferon response and cellular response to viral pathogens being upregulated at both time points and in both models (Figure 5 G–H, File S2). At 2 months post-treatment, the innate immune response was the most pronounced signature, especially in 5xFAD mice who had worse amyloid burden overall. Upregulated immune response genes included *Stat1* and *Stat2*, and genes regulated by *Stat1* and *Stat2*, such as oligo-adenylate synthase genes (*Oas1a*, *Oas1b*, *Oas1g*, *Oas2*, *Oas3*, *Oasl1*, *Oasl2*), interferon-related genes (*Irf7*, *Irf9*, *Stat1*, *Ifit1*, *Ifit2*, *Ifit3*, *Ifi27*, *Ifi35*, *Ifi44*), and cytokines/chemokines (*Ccl12*, *Ccl2*, *Ccl5*, *Cxcl10*, *Cxcl13*, *Cxcl16*, *Tnfsf13b*) (Figure 5I, Tables S6– and S7, File S2).[70] Upregulation of key immune-related genes *Lag3*, *Ccl5*, *Cxcl13*, *Oas3*, and *Lrf7* were confirmed with RTqPCR (Figure S6).

Apoe knockout induces more pronounced changes in inflammatory gene signatures in models of neurodegeneration than in the absence of disease (ie, wild-type animals), suggesting that *Apoe* silencing may not be the only factor driving inflammation.[71,72] Rather, the strong interferon signature associated with *Apoe* silencing might reflect underlying DAM or activated astrocytes.[45,73] Indeed, we observed a strong correlation between di-siRNA-*Apoe* treated 5xFAD mice and DAM expression signatures identified in single-cell RNA sequencing studies[40–42,45] (Figure 5J, Figure S7). Pearson correlation between *Apoe* and each DAM marker gene (Figure 4K) confirmed an overall inverse correlation with *Apoe* expression levels but also highlighted a small number of genes that are positively correlated with *Apoe* expression. In particular, *Aplp2* and *Apbb2*, two genes previously identified as being involved in APP processing, are significantly positively correlated with *Apoe* expression (File S4). Simultaneously, *Apoe* silencing increased expression of *C1qa* and *C1qb*, two key markers of homeostatic microglia.[73] Our data seem to contradict previous studies showing that genetic

1000 μm. (E) Aβ–42 using D9A3A in controls (left) and treated (right) animals. Scale bar: 1000 μm. (F) Zoom of cortical regions from panel D showing neuronal amyloid reactivity in both groups and reduction in amyloid plaque deposition in di-siRNA^{APOE} treated animals. Scale bar: 1000 μm. (G) Zoom of cortical regions from panel E showing Aβ42 plaque reduction in di-siRNA^{APOE} treated animals. Scale bar: 1000 μm. (H,I) Quantification of plaque burden measured as percent area, separated by sex using APP6E10 (H) and Aβ42 antibodies (I). (J,K) MSD quantification of insoluble amyloid in the cortex (J) and hippocampus (K). Statistics: *t*-test per brain region; sex separated; $n = 9–10$ per sex per group. Timepoint: 17 weeks old, 2 months post-injection. Aβ, amyloid beta; di-siRNA, divalent small interfering RNA; MSD, Meso Scale Discovery; NTC, non-targeting (vehicle) controls. $^{*}p < 0.0332$, $^{**}p < 0.0021$, $^{***}p < 0.0002$, $^{****}p < 0.0001$.

15525279, 2024, 4, Downloaded from https://alz-journals.onlinelibrary.wiley.com/doi/10.1002/alz.13703 by Cochrane Luxembourg, Wiley Online Library on [23/01/2026]. See the Terms and Conditions (https://onlinelibrary.wiley.com/terms-and-conditions) on Wiley Online Library for rules of use; OA articles are governed by the applicable Creative Commons License

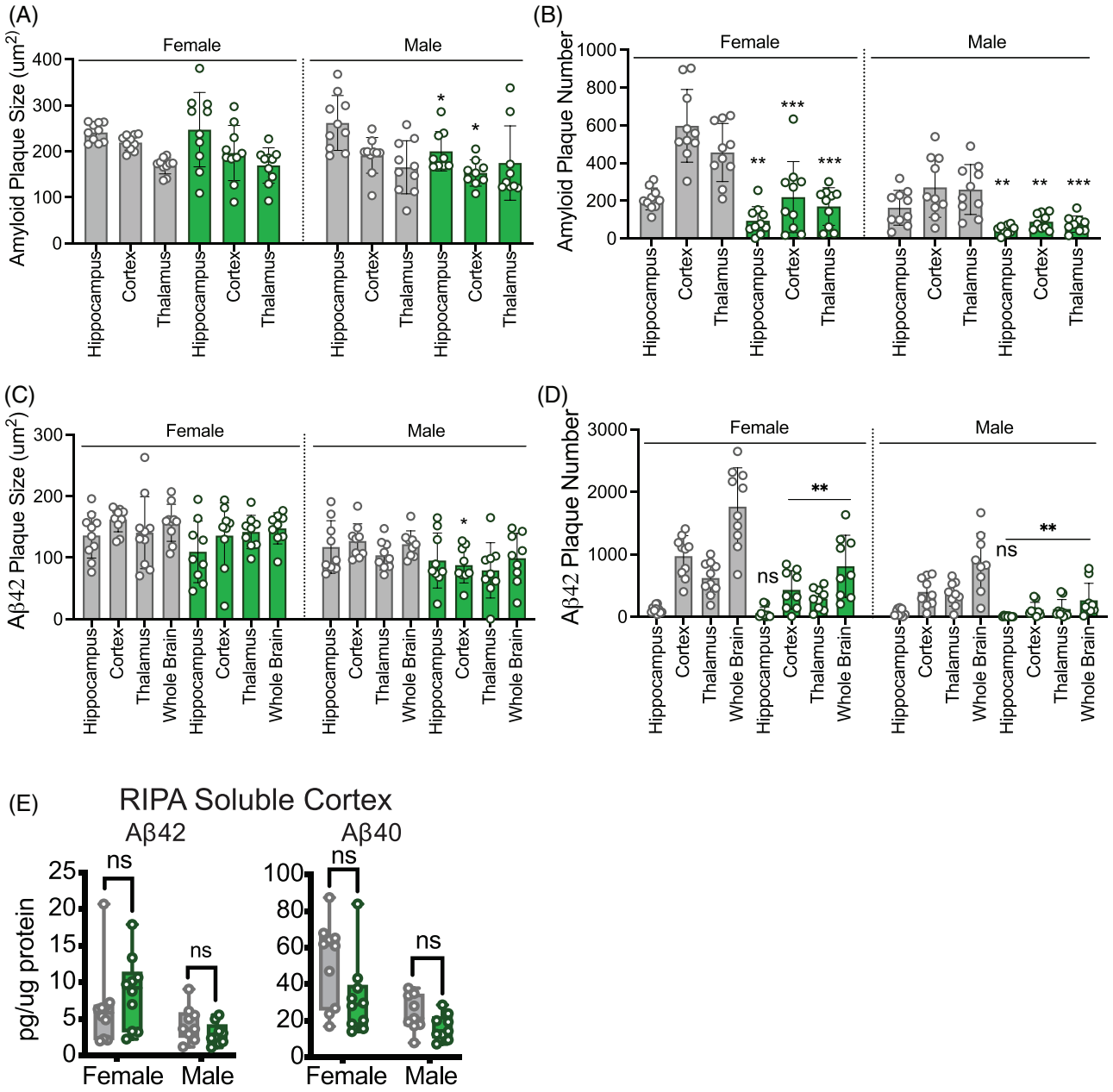

FIGURE 3 Silencing *Apoe* primarily reduces plaque number. (A) Amyloid plaque size, and (B) amyloid plaque number measured using APP6E10 antibody. (C) Aβ42 plaque size, and (D) Aβ42 plaque number measured using Aβ42-specific antibody (D9A3A) in 5xFAD treated and control mice, separated by sex. (E) MSD ELISA quantification of Aβ42 and Aβ40 in soluble brain fractions. Statistics: *t*-test per brain region; sex separated. Timepoint: 17 weeks old, 2 months post-injection (n = 9-10 per sex per group). Di-siRNA^{NTC} is shown in grey, and di-siRNA^{ApoE} is shown in green. Aβ, amyloid beta; ELISA, enzyme-linked immunosorbent assay; MSD, Meso Scale Discovery. $^{*}p < 0.0332$, $^{**}p < 0.0021$; $^{***}p < 0.0002$; $^{****}p < 0.0001$.

Apoe deficiency attenuates inflammatory signatures (reviewed in[74]), a discrepancy that could be related to the time point in disease progression at which the transcriptome was evaluated, or the time point of *Apoe* modulation (adulthood vs embryonic). Interestingly, expression profiles were positively associated with the microglial response to injecting Aβ/ApoE3 lipoprotein complex into wild-type mouse brain and negatively associated with the response to injecting Aβ/ApoE4 lipoprotein (Figure S7a).[42] These discrepancies highlight the important role single cell RNAseq (vs bulk performed here) can play in elucidating the nuances of expression profiles.

Pathways associated with axonogenesis, neurotransmitter transport, and synaptic organization were downregulated after silencing *Apoe* for 2 months in 5xFAD mice (Figure 6). However, signatures and components of the classical complement cascade (*C1qa*, *C1qb*) were upregulated, consistent with activation of synapse pruning and lysosomal activity in homeostatic microglia.[45,73,75] The absence of

15525279, 2024, 4, Downloaded from https://alz-journals.onlinelibrary.wiley.com/doi/10.1002/alz.13703 by Cochrane Luxembourg, Wiley Online Library on [23/01/2026]. See the Terms and Conditions (https://onlinelibrary.wiley.com/terms-and-conditions) on Wiley Online Library for rules of use; OA articles are governed by the applicable Creative Commons License

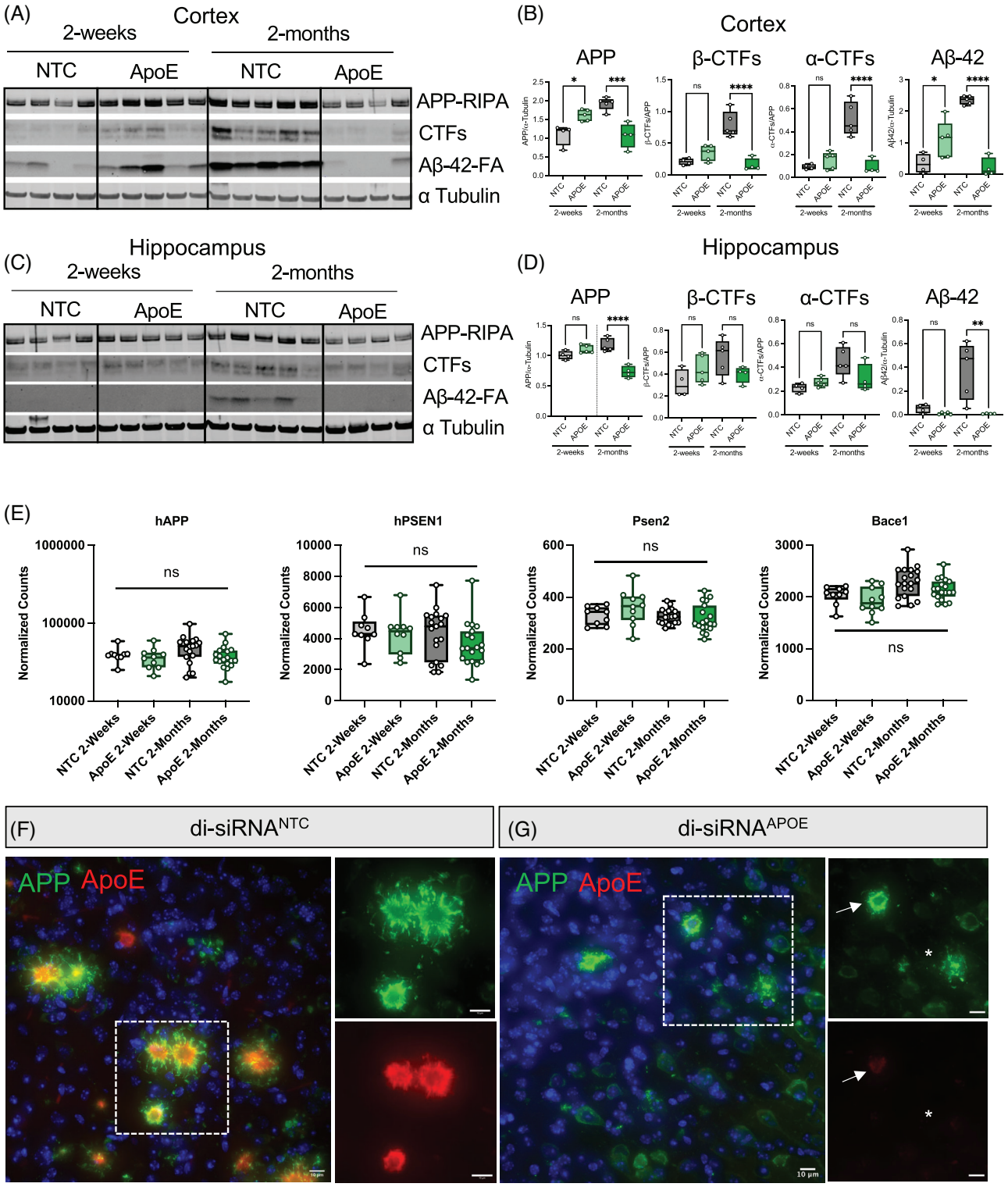

FIGURE 4 *Apoe* silencing decreases amyloid CTF production and removes structural support for amyloid plaques. Western blots (A) and quantification (B) showing a reduction in CTFs and Aβ42 in the cortex of treated compared to control animals. Western blots (C) and quantification (D) showing a reduction in APP and Aβ42 in the hippocampus of treated compared to control animals. $N = 4–5$ per group. Statistics: one-way ANOVA. (E) RNA expression levels of APP, PSEN1, PSEN2, and BACE1 in the cortex of treated and control animals. (F,G) Co-staining of amyloid plaques (APP6E10, green) and APOE (red) in control (F) and *Apoe* silenced (G) 5xFAD mice. Insets show amyloid (top, green) and APOE (red, bottom). Arrows denote early plaque with APOE present in the core while star denotes APOE poor plaque with altered structure. 63x, scale bar: 10 μm. Aβ, amyloid beta; APP, amyloid precursor protein; CTF, carboxy-terminal fragment; di-siRNA, divalent small interfering RNA; NTC, non-targeting (vehicle) controls; RIPA, radioimmunopreciptation assay. $^{*}p < 0.0332$, $^{**}p < 0.0021$, $^{***}p < 0.0002$, $^{****}p < 0.0001$.

15525279, 2024, 4, Downloaded from https://alz-journals.onlinelibrary.wiley.com/doi/10.1002/alz.13703 by Cochrane Luxembourg, Wiley Online Library on [23/01/2026]. See the Terms and Conditions (https://onlinelibrary.wiley.com/terms-and-conditions) on Wiley Online Library for rules of use; OA articles are governed by the applicable Creative Commons License

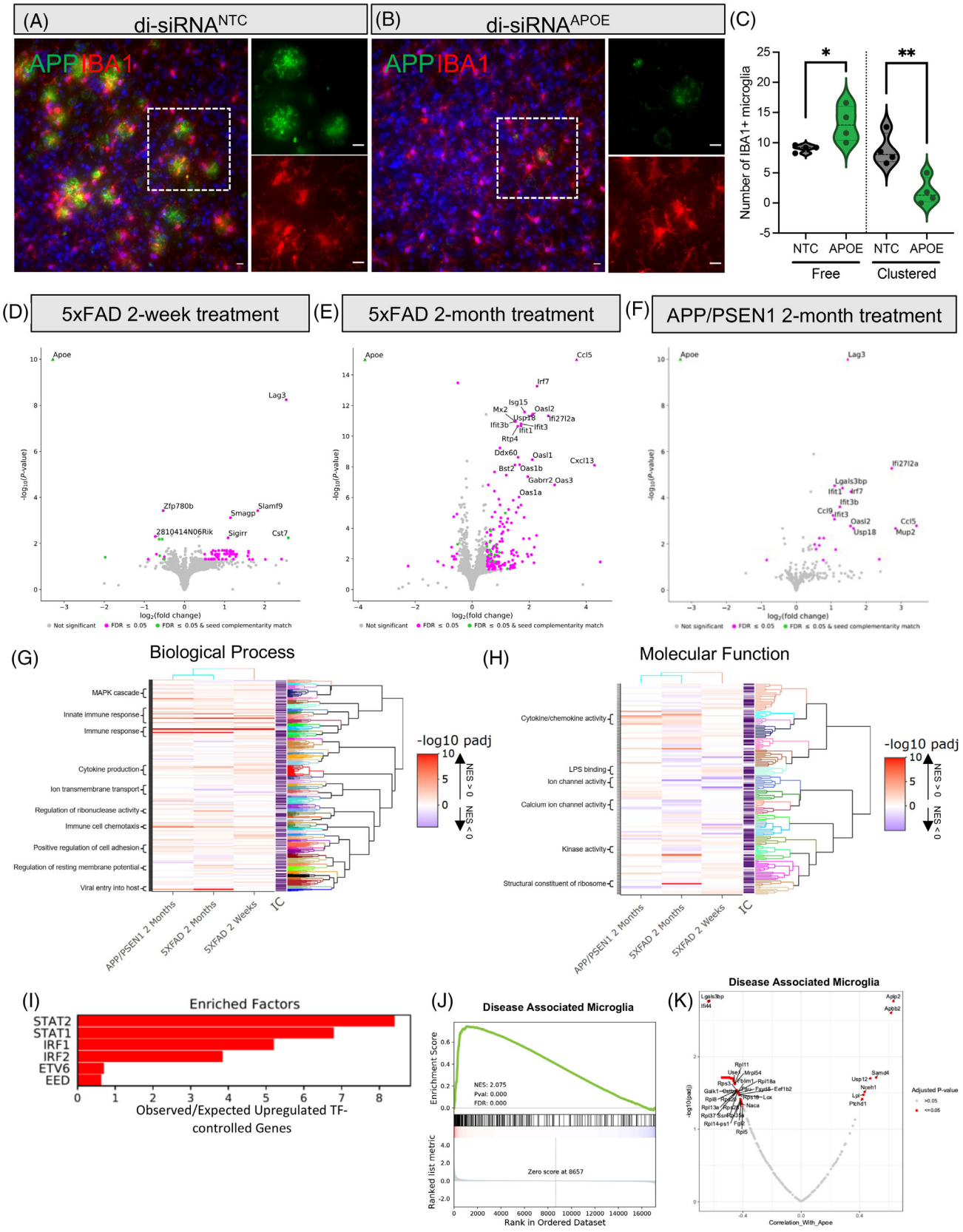

FIGURE 5 *Apoe* silencing activates the expression of immune-related pathways. Co-staining of amyloid plaques (APP, green) and microglia (IBA1, green) in control (A) and treated (B) 5xFAD mice. Insets show amyloid (top, green) and IBA1 (bottom, green). Representative images from corresponding cortex regions are shown. 40x, scale bar: 10 μm. (C) Quantification of IBA1+ cell clustering around amyloid plaques. Statistics: one-way ANOVA. (D–F) Volcano plots showing differentially expressed genes after two weeks (D) and 2 months (E) of *Apoe* silencing in 5xFAD

15525279, 2024, 4, Downloaded from https://alz-journals.onlinelibrary.wiley.com/doi/10.1002/alz.13703 by Cochrane Luxembourg, Wiley Online Library on [23/01/2026]. See the Terms and Conditions (https://onlinelibrary.wiley.com/terms-and-conditions) on Wiley Online Library for rules of use; OA articles are governed by the applicable Creative Commons License

these signatures in APP/PSEN1 mice, which showed lower overall amyloid burden, suggests that worsening disease pathology combined with *Apoe* silencing stimulates synapse pruning, which may serve to strengthen neurons in the context of worsening neurodegeneration.

Sex affects *Apoe*-related progression of AD. Nevertheless, transcriptional changes in response to *Apoe* silencing were similar in male and female mice, with ribosomal subunit protein genes being the exception (Figure S8a). Interferon genes were activated in both sexes, but the effect was stronger in male mice at 2 months post-injection (Figure S8a).

Interestingly, after silencing *Apoe* for 2 months in 5xFAD mice, we observed increased expression of other lipoproteins, including *ApoA1* (log2fold change = 0.79, $p = 0.0178$) and *ApoC1* (log2fold change = 0.86, $p = 0.003$), which could reflect a compensatory response to ensure proper lipid transport and cellular growth in the brain.[76,77] Taken together, silencing *Apoe* with therapeutic siRNAs is target specific, significantly modulates immune system processing, and slows plaque deposition throughout the brain.

3.7 | Gene network analysis identifies clusters associated with *Apoe* silencing over time in 5xFAD mice

Over time, *Apoe* silencing normalized the expression of 21 genes whose expression changed during disease progression, altered the expression of 129 other genes, and impacted GO pathways (Figure S8b,c). To further investigate how *Apoe* silencing alters disease-associated gene sets, we performed WGCNA in 5xFAD mice.[78] We identified WGCNA modules that positively or negatively correlated with amyloid burden (p-value < 0.05, absolute value of $R > 0.3$) (Figure 6A) and looked more closely at modules that were also significantly changed after silencing *Apoe*. The dark red and midnight blue modules were negatively correlated with amyloid burden and rescued by *Apoe* silencing (Figure 6C,D). The purple module was positively correlated with amyloid burden and downregulated by *Apoe* silencing (Figure 6E). These three modules were enriched for mitochondrial and electron transport chain genes (dark red), ribosomal subunit proteins, translation, and translational regulation (midnight blue), and synapse-related genes, including glutamatergic synapses, and predicted targets of mmu-miR-15a-5p and mmu-miR-425-5p (purple module). The gene ontologies associated with *Apoe* silencing are like those of *Apoe2* carriers, who have increased protection against AD.[79] The complete data set for the gene network analysis is shown in the file S3.

4 | DISCUSSION

The presence of *APOE4* is the strongest genetic risk factor for developing late-onset AD.[3,80,81] Some *APOE*-based therapeutics, including an *APOE* mimetic and adeno-associated virus (AAV) gene delivery of *APOE2*, are in Phase 1 clinical trials,[82] but many previously evaluated *APOE* therapies (eg, Bexarotene and Rosiglitazone) have been ineffective in humans, and none silence *APOE* to the levels seen in transgenic proof-of-concept studies.[82,83] Here, we effectively evaluate the spatial and functional relationships between systemic and CNS pools of *Apoe*, the impact of these pools on AD pathological phenotypes, and identify potential mechanisms through which *Apoe* impacts AD pathology. With a single administration of 237 μg di-siRNA, we achieved potent, sustained silencing of CNS *Apoe*, likely due to the integration of a fully-modified scaffold that allows the siRNA to be internalized by the cell and stored in the endosome for sustained release.[84] Importantly, ours is the first study to show that silencing *Apoe* with siRNAs can be therapeutic: silencing *Apoe* after the onset of cellular changes significantly reduced amyloid pathology in 5xFAD mice. Mechanistically, our findings suggest that, when present, *Apoe* modulates APP levels, serves as a scaffold for plaque formation, and prevents immune-mediated amyloid degradation, leading to microglial dysfunction and cellular death.[45,66,68] Moving forward, this study provides the rationale and technology necessary to further evaluate the relative impact of therapeutic *APOE* silencing on other neurodegenerative diseases, including Huntington's disease and tauopathies,[18] and to further explore *APOE* modulation as a therapeutic paradigm for AD. The therapeutic siRNAs developed in this study can be translated to potential clinical trials, accelerating development of much needed disease-modifying therapies.

Building on previous studies,[15,16] we found no detectable trafficking of non-fragmented *Apoe* in and out of the adult CNS, even after the removal of systemic *Apoe*. While silencing liver *Apoe* did not significantly improve amyloid phenotypes in APP/PSEN1 mice, we did observe a moderate, yet significant, increase in soluble cortical Aβ42. Even though only complete silencing of hepatic *Apoe* resulted in detectable changes in serum cholesterol levels, partial silencing seen with di-siRNAs may have other non-detectable impacts. Our results,

mice, and differentially expressed genes after 2 months of *Apoe* silencing in APP/PSEN1 mice (F). FDR set to < 0.05; shown in pink. Green denotes FDR < 0.05 and the presence of the seed match in the 3′UTR. Grey: not significant. Log2fold change cut-off set to 0.5 (+/-). (G,H) Gene set enrichment analysis on genes expressed in all conditions, clustered by gene set member semantic similarity. Labels indicate cluster themes. (I) Analysis of transcription factor target gene enrichment in upregulated genes at 2 months post-treatment in 5XFAD, using the MAGIC package. (J) Comparison of gene overlap between *Apoe* silencing for 2 months in 5XFAD and marker genes of disease-associated microglia from Keren-Shaul et al., 2017. (K) Volcano plot of Pearson correlation between each gene in the "Disease-Associated Microglia" marker gene set and *Apoe* in the 5XFAD mice 2 months post-injection. Mice: 5xFAD, Age: 11 and 17 weeks old. Timepoints: 2 weeks ($n = 9$–10/group) and 2 months ($n = 18$–20/group) post-injection. APP/PSEN1 mouse model: Age: 16 weeks old, 2 months post-injection. $N = 8$–10 per group. di-siRNA, divalent small interfering RNA; FDR, false discovery rate; NTC, non-targeting (vehicle) controls.

15525279, 2024, 4, Downloaded from https://alz-journals.onlinelibrary.wiley.com/doi/10.1002/alz.13703 by Cochrane Luxembourg, Wiley Online Library on [23/01/2026]. See the Terms and Conditions (https://onlinelibrary.wiley.com/terms-and-conditions) on Wiley Online Library for rules of use; OA articles are governed by the applicable Creative Commons License

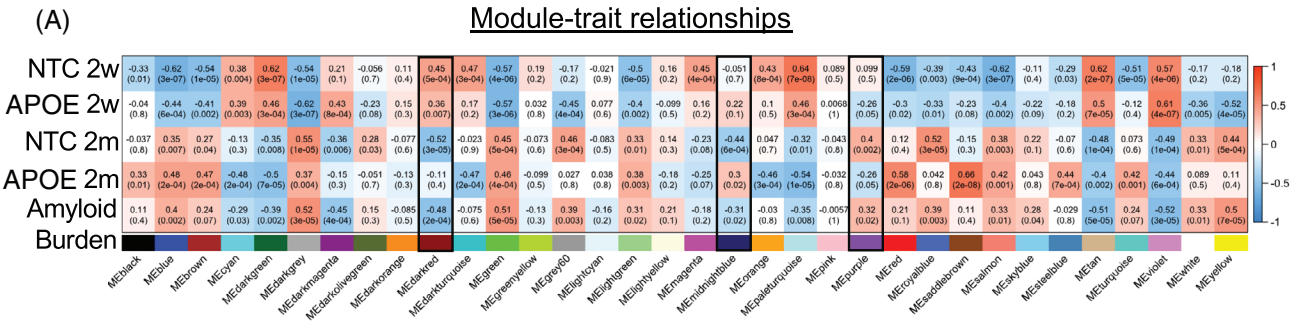

(B) Dark Red

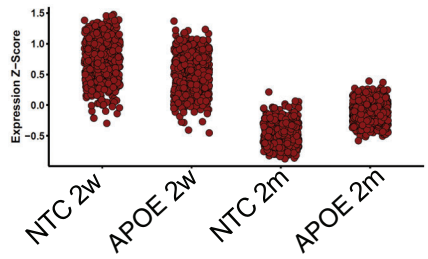

Ontology	Term	P Adj.
GO BP	electron transport chain	2.90E-16
GO BP	mitochondrial respiratory chain complex assembly	2.93E-14
GO CC	mitochondrial protein-containing complex	7.65E-30
GO CC	mitochondrion	8.30E-30
GO MF	electron transfer activity	2.54E-12
GO MF	NADH dehydrogenase (ubiquinone) activity	2.14E-06
Reactome	Respiratory electron transport, ATP synthesis by chemiosmotic coupling, and heat production by uncoupling proteins.	1.29E-23
Reactome	Respiratory electron transport	1.16E-21
Reactome	Mitochondrial translation elongation	3.82E-09

(C) Midnight Blue

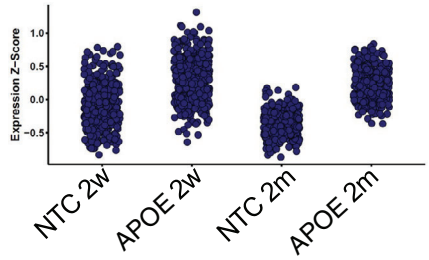

Ontology	Term	P Adj.
GO BP	translation	1.75E-18
GO BP	peptide metabolic process	1.75E-18
GO CC	cytosolic ribosome	9.17E-52
GO CC	ribosomal subunit	2.23E-39
GO MF	structural constituent of ribosome	6.44E-46
GO MF	structural molecule activity	8.24E-24
Reactome	SRP-dependent cotranslational protein targeting to membrane	4.84E-49
Reactome	Nonsense Mediated Decay (NMD) independent of the Exon Junction Complex (EJC)	1.12E-48
Reactome	Formation of a pool of free 40S subunits	5.32E-47

(D) Purple

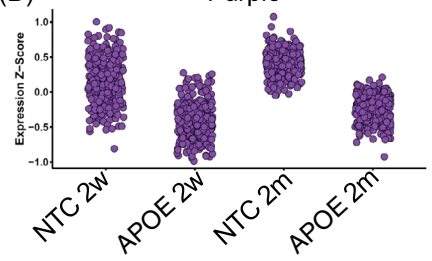

Ontology	Term	P Adj.
GO BP	chemical synaptic transmission	0.00108
GO BP	behavior	0.00108
GO BP	trans-synaptic signaling	0.00108
GO CC	synapse	3.25E-05
GO CC	postsynapse	0.00035
GO CC	membrane	0.00035
GO CC	glutamatergic synapse	0.0006
miRNA	mmu-miR-15a-5p	8.09E-06
miRNA	mmu-miR-425-5p	1.13E-05

FIGURE 6 *Apoe* silencing dynamically rescues gene expression alterations in 5xFAD mice. (A) Correlation between WGCNA clusters, treatment, and amyloid burden, measured as percent of brain area positive for amyloid IHC (see methods). (C–E) WGCNA module gene average expression z-score and gene ontology results for modules that are significantly correlated with amyloid burden and treatment conditions ($R > 0.3$, p-value < 0.05). 5xFAD mouse model; Age: 11 and 17 weeks old. Timepoints: 2 weeks post-injection ($n = 9–10$/group), 2 months post-injection ($n = 18–20$/group). IHC, immunohistochemistry; NTC, non-targeting (vehicle) controls; WGCNA, weighted gene co-expression network analysis.

among others, highlight the need to maintain systemic *Apoe* expression in therapeutic paradigms moving forward[85] and highlight an important area of focus as we continue to work on therapeutic strategies to selectively silence *Apoe* in the CNS.

Disease pathology drives *Apoe* expression in activated microglia, which may both promote plaque formation via post-translational modification and enhance disease-associated inflammation.[45,73] Consistent with prior reports, we also found that *Apoe* serves as a key modulator of immune response pathways in AD.[45,66,86–88] However, unlike many studies, we observed that silencing *Apoe* promoted the expression of genes involved in immune response pathways. The data demonstrating immune activation upon *Apoe* silencing is seen only with *Apoe*-targeting

15525279, 2024, 4, Downloaded from https://alz-journals.onlinelibrary.wiley.com/doi/10.1002/alz.13703 by Cochrane Luxembourg, Wiley Online Library on [23/01/2026]. See the Terms and Conditions (https://onlinelibrary.wiley.com/terms-and-conditions) on Wiley Online Library for rules of use; OA articles are governed by the applicable Creative Commons License

siRNAs and not identified in the context of non-targeting siRNAs of identical chemical configuration, administered using the same methods, side-by-side. While using a single *Apoe*-specific compound could not completely rule out the effects being sequence-specific, it is highly unlikely. The observed signature is like the one observed in orthogonal animal models, where *Apoe* is removed genetically. In addition, the signature is time dependent, taking 2 months and not present after 2 weeks, which is more consistent with gene-specific, rather than non-specific, effects. Although we did not perform cell-type-specific RNAseq, expression signatures after silencing *Apoe* resembled those seen in DAM cells. Microglial responses in AD are dynamic: DAM have been implicated in acute inflammation required to acutely clear toxic pathogens, as well as chronic, possibly harmful, inflammatory processes.[89] Given their dynamic nature, it is difficult to draw conclusions regarding the implications of DAM expression signatures, and at what point the switch between acute and chronic activation occurs. It is possible that silencing *Apoe* slows the turning point from acute to chronic neuroinflammation in the context of AD.[90] Whether the responses observed after silencing *Apoe* correspond with protective acute immune responses or chronic inflammatory signaling warrants further investigation.[45,91]

The *Apoe*-dependent reduction in APP and amyloid CTFs we observed was surprising, particularly as there was no effect on the expression of APP mRNA or APP processing machinery (*APP*, *BACE1*, *PSEN*). Silencing *Apoe* may reduce APP stability, may increase CTF degradation, or may decrease CTF production. Changes in production could be due to *Apoe*-dependent changes in APP membrane localization and cellular trafficking.[92–94] In addition, silencing *Apoe* led to a reduction in APOE-rich amyloid cores, which may reduce the stability of amyloid plaques and allow for effective immune-related clearance of toxic proteins. We observed an interesting increase in CTFs after 2 weeks that was reversed after 2 months of *Apoe* silencing, providing some insight into the necessary timing and duration of treatment. While in these studies we treated at only one time point, future studies treating at different time points and for varying durations are necessary to further understand the potential therapeutic paradigm and impact of *Apoe* silencing on the kinetics of CTF production.

A major caveat to the applicability of our results is the known differences in the structure, binding ability, and impact on disease between mouse and human *APOE*, as well as the three human *APOE* isoforms. For example, *APOE* isoforms differentially drive plaque formation and vascular pathology that contribute to Alzheimer's disease progression.[95,96] In both mouse and human samples, *APOE* isoforms contribute differently to the formation of fibrillar, versus dense core versus vascular amyloid, potentially limiting the applicability of our results, which focused on mouse *Apoe* in 5xFAD, to human disease. Given the structural and binding differences between *APOE* isoforms, future studies evaluating the impact of silencing *APOE* with siRNAs in models with other *APOE* variants are warranted.

The role of *APOE* in AD has been muddled by differences in conferred risk between populations (ie, Asian, European, African American),[97–100] and confounded by factors like body mass index (BMI) and diabetes. GWAS studies point towards a protective role of *APOE2*,[101] and in vivo analyses suggest gain-of-function toxicity for *APOE4*.[101,102] In support of the gain-of-function model, individuals heterozygous for *APOE4* (eg, *APOE2/4* or *APOE3/4*) have similar rates of Aβ burden, suggesting that the toxicity of *APOE4* outweighs a protective role for *APOE2*.[83] Similarly, our results support a toxic gain-of-function effect of *Apoe* on both amyloid plaque formation and immune dysregulation.

Would *APOE* silencing in adults be a safe therapeutic approach? Although CNS apoE is involved in synapse formation and neurite growth[103] (reviewed in[104]), individuals null for *APOE* are cognitively normal.[105,106] Our results indicated that silencing *Apoe* downregulates pathways involved in axonogenesis and synaptic organization, which may impact neuronal viability. Interestingly, *APOE2* also shows reduced synapse formation despite being protective against AD,[107] and our comparison with published datasets demonstrates similar expression profiles between *APOE2* and *Apoe*-silenced samples. Prior studies have shown that decreased cholesterol and cellular binding underlies the protective benefit of the *APOE2* allele and other *APOE* mutations,[102,108,109] suggesting that silencing *APOE3* and *APOE4* for short periods during adulthood, thus reducing binding, may phenocopy the protective *APOE*2 state. Although a reduction in Aβ plaques correlates well with behavioral improvements in prior studies,[110] we did not investigate the impact of silencing *Apoe* on AD-related cognitive dysfunction in these experiments, because neither the 5xFAD nor APP/PSEN1 models develop cognitive deficits until at least 6 months of age, and the results can be highly variable.[111,112] We did, however, confirm that silencing *Apoe* with di-siRNA for extended periods does not negatively affect cognition in young-adult 5xFAD mice, and thus, appears to be well-tolerated and the impact on disease-related cognition worth pursuing further. Additional studies involving additional dosing regimens for long-term modulation of *Apoe* are required to evaluate the potential impact of the *Apoe* modulation, plaque clearance, and increase in glia activation on behavioral phenotypes.

Here, we developed translational tools that potently modulate *APOE* in the context of late-onset AD. These novel tools enable the future investigation of outstanding questions and aid in the development of desperately needed disease modifying therapeutics for AD and other conditions in which *APOE* plays a contributory role.

AUTHOR CONTRIBUTIONS

Chantal M. Ferguson, Anastasia Khvorova, and Evgeny Rogaev conceived of the project. Chantal M. Ferguson and Anastasia Khvorova contributed to the experimental design. Chantal M. Ferguson, Bruno M. D. C Godinho, and Andrew Coles performed ICV injections. Chantal M. Ferguson and Anastasia Grigorenko performed mouse breeding. Chantal M. Ferguson, Julianna Buchwald, Francesco Santarelli, and Michael T. Heneka performed sample preparation and analysis. Samuel Hildebrand performed RNA seq analysis. Dimas Echeverria, Matthew R. Hassler, Lorenc Vangjeli, Jacquelyn Sousa, and Nicholas McHugh synthesized compounds. Chantal M. Ferguson, Samuel Hildebrand, and Anastasia Khvorova wrote the manuscript.

15525279, 2024, 4, Downloaded from https://alz-journals.onlinelibrary.wiley.com/doi/10.1002/alz.13703 by Cochrane Luxembourg, Wiley Online Library on [23/01/2026]. See the Terms and Conditions (https://onlinelibrary.wiley.com/terms-and-conditions) on Wiley Online Library for rules of use; OA articles are governed by the applicable Creative Commons License

ACKNOWLEDGMENTS

We would like to thank Dr Arya Biragyn, NIA, for gifting us AD mouse strains, and the Animal Medicine Group at UMass Chan Medical School. We would like to thank Emily Haberlin and Darryl Conte for editing the manuscript. This work was supported by NS 104022, GM-131839, S10 OD020012, and ADDF 20170101/Rogaev; National Research Service Award 1F30AG066373-01, and T32GM107000.

CONFLICT OF INTEREST STATEMENT

Chantal Ferguson, Evgeny Rogaev, and Anastasia Khvorova hold patent applications for the human ApoE targeting siRNA sequences. U.S. Patent Application Serial No. 16/818,563. March 13, 2020. Patent pending. Samuel Hildebrand, Bruno M.D.C Godinho, Julianna Buchwald, Dimas Echeverria, Andrew Coles, Anastasia Grigorenko, Lorenc Vangjeli, Jacquelyn Sousa, Nicholas McHugh, Matthew Hassler, Francesco Santarelli, Michael T. Heneka declare no competing interests. Author disclosures are available in the supporting information.

DATA AVAILABILITY STATEMENT

All data generated during this study are either included in this article or are available from the corresponding author on reasonable request. Raw and processed RNA sequencing data was uploaded to the Gene Expression Omnibus (GSE186756). Custom scripts used for RNA sequencing analysis have been deposited to https://github.com/shildebr12/Ferguson_et_al_2021.

CONSENT STATEMENT

Consent was not necessary as human subjects were not involved.

ETHICS STATEMENT

All experimental studies involving animals were approved by the University of Massachusetts Medical School Institutional Animal Care and Use Committee (IACUC Protocols #A-2411 and #A-1744) and performed according to the guidelines and regulations therein described.

ORCID

Chantal M. Ferguson https://orcid.org/0000-0002-9442-1249

REFERENCES

1. Qaseem A, Snow V. Owens, and the Joint American College of Physicians/American Academy of Family Physicians Panel on dementia. Current pharmacologic treatment of dementia: a clinical practice guideline from the American College of Physicians and the American academy of family physicians. *Ann Intern Med*. 2008;148:370-378.
2. Trinh NH, Hoblyn J, Mohanty S, Yaffe K. Efficacy of cholinesterase inhibitors in the treatment of neuropsychiatric symptoms and functional impairment in Alzheimer disease. *JAMA*. 2003;289:210-216.
3. Corder EH, Saunders AM, Strittmatter WJ, et al. Gene dose of apolipoprotein E Type 4 Allele and the risk fo Alzheimer's disease in late onset families. *Science*. 1993;261:921-923.
4. Frisoni GB, Govoni S, Geroldi C, et al. Gene dose of the E4 Allele of apolipoprotein E and disease progression in sporadic late-onset Alzheimer's disease. *Ann Neurol*. 1995;37:596-604.
5. Karch CM, Goate AM. Alzheimer's disease risk genes and mechanisms of disease pathogenesis. *Biol Psychiatry*. 2015;77:43-51.
6. Pitas RE, Boyles JK, Lee SH, Hui D, Weisgraber KH. Lipoproteins and their receptors in the central nervous system. *J Biol Chem*. 1987;262:14352-14360.
7. Xu Q, Bernardo A, Walker D, Kanegawa T, Mahley RW, Huang Y. Profile and regulation of apolipoprotein E (ApoE) expression in the CNS in mice with targeting of green flourescent protein gene to teh ApoE locus. *Neurobiol Dis*. 2006;26:4985-4994.
8. Michael S, Brown JLG. A receptor-mediated pathway for cholesterol homeostasis. *Science*. 1986;232:34-47.
9. Innerarity RWMaTL. Lipoprotein receptors and cholesterol homeostasis. *Biochim Biophys Acta*. 1983;737:197-222.
10. David M, Holtzman KRB, Tenkova T, et al. Apolipoprotein E isoform-dependent amyloid deposition and neuritic degeneration in a mouse model of Alzheimer's disease. *Proc Natl Acad Sci*. 2000;97:2892-2897.
11. David M, Holtzman KRB, Wu S, et al. Expression of human apolipoprotein E reduces amyloid-β deposition in a mouse model of Alzheimer's disease. *J Clin Invest*. 1999;103:15-21.
12. Kim J, Jiang H, Park S, et al. Haploinsufficiency of human APOE reduces amyloid deposition in a mouse model of amyloid-beta amyloidosis. *J Neurosci*. 2011;31:18007-18012.
13. Bales KR, Verina T, Dodel RC, et al. Lack of apolipoprotein E dramatically reduces amyloid β-peptide deposition. *Nat Genet*. 1997;17:263-264.
14. Zhang SH, Reddick RL, Piedrahita JA, Maeda N. Spontaneous hypercholesterolemia and arterial lesionsinmicelackingapolipoproteinE. *Science*. 1992;258:468-471.
15. Lane-Donovan C, Wong WM, Durakoglugil MS, et al. Genetic restoration of plasma ApoE improves cognition and partially restores synaptic defects in ApoE-deficient mice. *J Neurosci*. 2016;36:10141-10150.
16. Huynh TV, Wang C, Tran AC, et al. Lack of hepatic apoE does not influence early Abeta deposition: observations from a new APOE knock-in model. *Mol Neurodegener*. 2019;14:37.
17. Huynh TV, Liao F, Francis CM, et al. Age-dependent effects of apoe reduction using antisense oligonucleotides in a model of beta-amyloidosis. *Neuron*. 2017;96:1013-1023. e4.
18. Litvinchuk A, Huynh TPV, Shi Y, et al. Apolipoprotein E4 reduction with antisense oligonucleotides decreases neurodegeneration in a tauopathy model. *Ann Neurol*. 2021;89(5):952-966.
19. Khvorova A, Watts JK. The chemical evolution of oligonucleotide therapies of clinical utility. *Nat Biotechnol*. 2017;35:238-248.
20. Akinc A, Querbes W, De S, et al. Targeted delivery of RNAi therapeutics with endogenous and exogenous ligand-based mechanisms. *Mol Ther*. 2010;18:1357-1364.
21. Nair JK, Willoughby JL, Chan A, et al. Multivalent N-acetylgalactosamine-conjugated siRNA localizes in hepatocytes and elicits robust RNAi-mediated gene silencing. *J Am Chem Soc*. 2014;136:16958-16961.
22. Nair JK, Attarwala H, Sehgal A, et al. Impact of enhanced metabolic stability on pharmacokinetics and pharmacodynamics of GalNAc-siRNA conjugates. *Nucleic Acids Res*. 2017;45:10969-10977.
23. Ray KK, Landmesser U, Leiter LA, et al. Inclisiran in patients at high cardiovascular risk with elevated LDL cholesterol. *N Engl J Med*. 2017;376:1430-1440.
24. Alterman JF, Godinho B, Hassler MR, et al. A divalent siRNA chemical scaffold for potent and sustained modulation of gene expression throughout the central nervous system. *Nat Biotechnol*. 2019;37:884-894.
25. Sharma VK, Osborn MF, Hassler MR, et al. Novel cluster and monomer-based GalNAc structures induce effective uptake of siRNAs in vitro and in vivo. *Bioconjug Chem*. 2018;29:2478-2488.
26. Haraszti RA, Roux L, Coles AH, et al. 5′-Vinylphosphonate improves tissue accumulation and efficacy of conjugated siRNAs in vivo. *Nucleic Acids Res*. 2017;45:7581-7592.

15525279, 2024, 4, Downloaded from https://alz-journals.onlinelibrary.wiley.com/doi/10.1002/alz.13703 by Cochrane Luxembourg, Wiley Online Library on [23/01/2026]. See the Terms and Conditions (https://onlinelibrary.wiley.com/terms-and-conditions) on Wiley Online Library for rules of use; OA articles are governed by the applicable Creative Commons License

27. Gentalen ET, Proctor JM. Using the peggy simple western system for fine needle aspirate analysis. *Methods Mol Biol*. 2015;1219:139-155. doi:10.1007/978-1-4939-1661-0_11
28. Venegas C, Kumar S, Franklin BS, et al. Microglia-derived ASC specks cross-seed amyloid-β in Alzheimer's disease. *Nature*. 2017;552:355-361.
29. Liu C, Desikan R, Ying Z, et al. Effects of a novel pharmacologic inhibitor of myeloperoxidase in a mouse atherosclerosis model. *PLoS One*. 2012;7:e50767.
30. Dobin A, Davis CA, Schlesinger F, et al. STAR: ultrafast universal RNA-seq aligner. *Bioinformatics*. 2013;29:15-21.
31. Li B, Dewey CN. RSEM: accurate transcript quantification from RNA-Seq data with or without a reference genome. *BMC Bioinf*. 2011;12:323.
32. Love MI, Huber W, Anders S. Moderated estimation of fold change and dispersion for RNA-seq data with DESeq2. *Genome Biol*. 2014;15:550.
33. Zhu A, Ibrahim JG, Love MI. Heavy-tailed prior distributions for sequence count data: removing the noise and preserving large differences. *Bioinformatics*. 2019;35:2084-2092.
34. Gennady K, Vladimir S, Nikolay B, Boris S, Maxim NA, Alexey S. Fast gene set enrichment analysis. *bioRxiv*. 2021:060012.
35. Brionne A, Juanchich A, Hennequet-Antier C. ViSEAGO: a bioconductor package for clustering biological functions using gene ontology and semantic similarity. *BioData Mining*. 2019;12:16.
36. Langfelder P, Horvath S. WGCNA: an R package for weighted correlation network analysis. *BMC Bioinf*. 2008;9:559.
37. Zhang Y, Parmigiani G, Johnson WE. ComBat-seq: batch effect adjustment for RNA-seq count data. *NAR Genom Bioinform*. 2020;2:lqaa078.
38. Botía JA, Vandrovcova J, Forabosco P, et al. An additional k-means clustering step improves the biological features of WGCNA gene co-expression networks. *BMC Syst Biol*. 2017;11:47.
39. Kolberg L, Raudvere U, Kuzmin I, Vilo J, Peterson H. gprofiler2 – an R package for gene list functional enrichment analysis and namespace conversion toolset g:profiler. *F1000Research*. 2020;9:709.
40. Mathys H, Adaikkan C, Gao F, et al. Temporal tracking of microglia activation in neurodegeneration at single-cell resolution. *Cell Rep*. 2017;21:366-380.
41. Hasel P, Rose IVL, Sadick JS, Kim RD, Liddelow SA. Neuroinflammatory astrocyte subtypes in the mouse brain. *Nat Neurosci*. 2021;24(10):1475-1487.
42. Fitz NF, Nam KN, Wolfe CM, et al. Phospholipids of APOE lipoproteins activate microglia in an isoform-specific manner in preclinical models of Alzheimer's disease. *Nat Commun*. 2021;12:3416.
43. Grubman A, Choo XY, Chew G, et al. Transcriptional signature in microglia associated with Abeta plaque phagocytosis. *Nat Commun*. 2021;12:3015.
44. Roopra A. MAGIC: a tool for predicting transcription factors and cofactors driving gene sets using ENCODE data. *PLoS Comput Biol*. 2020;16:e1007800.
45. Sala Frigerio C, Wolfs L, Fattorelli N, et al. The major risk factors for Alzheimer's disease: age, sex, and genes modulate the microglia response to abeta plaques. *Cell Rep*. 2019;27:1293-1306 e6.
46. Butler A, Hoffman P, Smibert P, Papalexi E, Satija R. Integrating single-cell transcriptomic data across different conditions, technologies, and species. *Nat Biotechnol*. 2018;36:411-420.
47. Ferguson CM, Echeverria D, Hassler M, Ly S, Khvorova A. Cell type impacts accessibility of mRNA to silencing by RNA interference. *Mol Ther Nucleic Acids*. 2020;21:384-393.
48. Garcia-Alloza M, Robbins EM, Zhang-Nunes SX, et al. Characterization of amyloid deposition in the APPswe/PS1dE9 mouse model of Alzheimer disease. *Neurobiol Dis*. 2006;24:516-524.
49. Jankowsky JLSH, Ratovitski T, Jenkins NA, Copeland NG, Borchelt DR. Co-expression of multiple transgenes in mouse CNS: a comparison of strategies. *Biomol Engineering*. 2001;16:157-165.
50. Jankowsky JL, Fadale DJ, Anderson J, et al. Mutant presenilins specifically elevate the levels of the 42 residue beta-amyloid peptide in vivo: evidence for augmentation of a 42-specific gamma secretase. *Hum Mol Genet*. 2004;13:159-170.
51. Ikonomovic MD, Abrahamson EE, Isanski BA, et al. X-34 labeling of abnormal protein aggregates during the progression of Alzheimer's disease *Methods Enzymol*. 2006;412:123-144. doi:10.1016/S0076-6879(06)12009-1
52. Ordonez-Gutierrez L, Fernandez-Perez I, Herrera JL, Anton M, Benito-Cuesta I, Wandosell F. AbetaPP/PS1 transgenic mice show sex differences in the cerebellum associated with aging. *J Alzheimers Dis*. 2016;54:645-656.
53. Gu L, Guo Z. Alzheimer's Abeta42 and Abeta40 peptides form interlaced amyloid fibrils. *J Neurochem*. 2013;126:305-311.
54. Esparza TJ, Wildburger NC, Jiang H, et al. Soluble amyloid-beta aggregates from human Alzheimer's disease brains. *Sci Rep*. 2016;6:38187.
55. Han S, Kollmer M, Markx D, Claus S, Walther P, Fandrich M. Amyloid plaque structure and cell surface interactions of beta-amyloid fibrils revealed by electron tomography. *Sci Rep*. 2017;7:43577.
56. Oakley H, Cole SL, Logan S, et al. Intraneuronal beta-amyloid aggregates, neurodegeneration, and neuron loss in transgenic mice with five familial Alzheimer's disease mutations: potential factors in amyloid plaque formation. *J Neurosci*. 2006;26:10129-10140.
57. Youmans KL, Tai LM, Kanekiyo T, et al. Intraneuronal Aβ detection in 5xFAD mice by a new Aβ-specific antibody. *Mol Neurodegener*. 2012;7:8.
58. Kummer MP, Heneka MT. Truncated and modified amyloid-beta species. *Alzheimers Res Ther*. 2014;6:28.
59. Miners JS, Barua N, Kehoe PG, Gill S, Love S. Aβ-Degrading enzymes: potential for treatment of Alzheimer disease. *J Neuropathol Exp Neurol*. 2011;70:944-959.
60. Leissring MA, Farris W, Chang AY, et al. Enhanced proteolysis of β-Amyloid in APP transgenic mice prevents plaque formation, secondary pathology, and premature death. *Neuron*. 2003;40:1087-1093.
61. Haass C, Kaether C, Thinakaran G, Sisodia S. Trafficking and proteolytic processing of APP. *Cold Spring Harb Perspect Med*. 2012;2:a006270.
62. Kiskis J, Fink H, Nyberg L, Thyr J, Li JY, Enejder A. Plaque-associated lipids in Alzheimer's diseased brain tissue visualized by nonlinear microscopy. *Sci Rep*. 2015;5:13489.
63. Hashimoto T, Serrano-Pozo A, Hori Y, et al. Apolipoprotein E, Especially Apolipoprotein E4, Increases the Oligomerization of Amyloid Peptide. *J Neurosci*. 2012;32:15181-15192.
64. Meilandt WJ, Ngu H, Gogineni A, et al. Trem2 deletion reduces late-stage Amyloid plaque accumulation, elevates the Abeta42:abeta40 Ratio, and exacerbates axonal dystrophy and dendritic spine loss in the PS2APP Alzheimer's mouse model. *J Neurosci*. 2020;40:1956-1974.
65. Parhizkar S, Arzberger T, Brendel M, et al. Loss of TREM2 function increases amyloid seeding but reduces plaque-associated ApoE. *Nat Neurosci*. 2019;22:191-204.
66. Ulrich JD, Ulland TK, Mahan TE, et al. ApoE facilitates the microglial response to amyloid plaque pathology. *J Exp Med*. 2018;215:1047-1058.
67. Stephen TL, Cacciottolo M, Balu D, et al. APOE genotype and sex affect microglial interactions with plaques in Alzheimer's disease mice. *Acta Neuropathol Commun*. 2019;7:82.

15525279, 2024, 4, Downloaded from https://alz-journals.onlinelibrary.wiley.com/doi/10.1002/alz.13703 by Cochrane Luxembourg, Wiley Online Library on [23/01/2026]. See the Terms and Conditions (https://onlinelibrary.wiley.com/terms-and-conditions) on Wiley Online Library for rules of use; OA articles are governed by the applicable Creative Commons License

68. Fitz NF, Wolfe CM, Playso BE, et al. Trem2 deficiency differentially affects phenotype and transcriptome of human APOE3 and APOE4 mice. *Mol Neurodegener*. 2020;15:41.
69. Rapic S, Backes H, Viel T, et al. Imaging microglial activation and glucose consumption in a mouse model of Alzheimer's disease. *Neurobiol Aging*. 2013;34:351-354.
70. Platanias LC. Mechanisms of type-I- and type-II-interferon-mediated signalling. *Nat Rev Immunol*. 2005;5:375-386.
71. Pandey RS, Graham L, Uyar A, Preuss C, Howell GR, Carter GW. Genetic perturbations of disease risk genes in mice capture transcriptomic signatures of late-onset Alzheimer's disease. *Mol Neurodegener*. 2019;14:50.
72. Shi Y, Yamada K, Liddelow SA, et al. ApoE4 markedly exacerbates tau-mediated neurodegeneration in a mouse model of tauopathy. *Nature*. 2017;549:523-527.
73. Keren-Shaul H, Spinrad A, Weiner A, et al. A unique microglia type associated with restricting development of Alzheimer's disease. *Cell*. 2017;169:1276-1290 e17.
74. Shi Y, Holtzman DM. Interplay between innate immunity and Alzheimer disease: aPOE and TREM2 in the spotlight. *Nat Rev Immunol*. 2018;18:759-772.
75. Chung WS, Verghese PB, Chakraborty C, et al. Novel allele-dependent role for APOE in controlling the rate of synapse pruning by astrocytes. *Proc Natl Acad Sci USA*. 2016;113:10186-10191.
76. Lewis TL, Cao D, Lu H, et al. Overexpression of human apolipoprotein A-I preserves cognitive function and attenuates neuroinflammation and cerebral amyloid angiopathy in a mouse model of Alzheimer disease. *J Biol Chem*. 2010;285:36958-36968.
77. Lefterov I, Fitz NF, Cronican AA, et al. Apolipoprotein A-I deficiency increases cerebral Amyloid Angiopathy and Cognitive Deficits in APP/PS1ΔE9 Mice. *J Biol Chem*. 2010;285:36945-36957.
78. Androvic P, Kirdajova D, Tureckova J, et al. Decoding the transcriptional response to ischemic stroke in young and aged mouse brain. *Cell Rep*. 2020;31:107777.
79. Hernandez-Ortega K, Garcia-Esparcia P, Gil L, Lucas JJ, Ferrer I. Altered machinery of protein synthesis in Alzheimer's: from the nucleolus to the ribosome. *Brain Pathol*. 2016;26:593-605.
80. Yu JT, Tan L, Hardy J. Apolipoprotein E in Alzheimer's disease: an update. *Annu Rev Neurosci*. 2014;37:79-100.
81. Hardy J, Escott-Price V. Genes, pathways and risk prediction in Alzheimer's disease. *Hum Mol Genet*. 2019;28:R235-R240.
82. Williams T, Borchelt DR, Chakrabarty P. Therapeutic approaches targeting Apolipoprotein E function in Alzheimer's disease. *Mol Neurodegener*. 2020;15:8.
83. Yamazaki Y, Zhao N, Caulfield TR, Liu CC, Bu G. Apolipoprotein E and Alzheimer disease: pathobiology and targeting strategies. *Nat Rev Neurol*. 2019;15:501-518.
84. Brown CR, Gupta S, Qin J, et al. Investigating the pharmacodynamic durability of GalNAc-siRNA conjugates. *Nucleic Acids Res*. 2020;48(21):11827-11844.
85. Giannisis A, Patra K, Edlund AK, et al. Brain integrity is altered by hepatic APOE ε4 in humanized-liver mice. *Mol Psychiatry*. 2022;27(8):3533-3543.
86. Krasemann S, Madore C, Cialic R, et al. The TREM2-APOE pathway drives the transcriptional phenotype of dysfunctional microglia in neurodegenerative diseases. *Immunity*. 2017;47:566-581 e9.
87. Wan YW, Al-Ouran R, Mangleburg CG, et al. Meta-Analysis of the Alzheimer's disease human brain transcriptome and functional dissection in mouse models. *Cell Rep*. 2020;32:107908.
88. Wang N, Wang M, Jeevaratnam S, et al. Opposing effects of apoE2 and apoE4 on microglial activation and lipid metabolism in response to demyelination. *Molecular Neurodegeneration*. 2022;17:75.
89. Sarlus H, Heneka MT. Microglia in Alzheimer's disease. *J Clin Invest*. 2017;127:3240-3249.
90. Friker LL, Scheiblich H, Hochheiser IV, et al. β-Amyloid Clustering around ASC fibrils boosts its toxicity in microglia. *Cell Rep*. 2020;30:3743-3754. e6.
91. Pascoal TA, Benedet AL, Ashton NJ, et al. Microglial activation and tau propagate jointly across Braak stages. *Nat Med*. 2021;27:1592-1599.
92. Wang H, Kulas JA, Wang C, Holtzman DM, Ferris HA, Hansen SB. Regulation of beta-amyloid production in neurons by astrocyte-derived cholesterol. *Proc Natl Acad Sci USA*. 2021;118:e2102191118.
93. Ye S, Huang Y, Mullendorff K, et al. Apolipoprotein (apo) E4 enhances amyloid beta peptide production in cultured neuronal cells: apoE structure as a potential therapeutic target. *Proc Natl Acad Sci USA*. 2005;102:18700-18705.
94. Paradise V, Sabu M, Bafia J, et al. ApoE isoforms differentially regulate neuronal membrane proteasomes to shift the threshold for pathological aggregation of endogenous Tau. *Biorxiv*. 2022:20221129518293.
95. Liao F, Zhang TJ, Jiang H, et al. Murine versus human apolipoprotein E4: differential facilitation of and co-localization in cerebral amyloid angiopathy and amyloid plaques in APP transgenic mouse models. *Acta Neuropathol Commun*. 2015;3:70.
96. Caesar I, Nilsson KPR, Hammarstrom P, et al. ApoE Alzheimer's Disease Aβ-amyloid plaque morphology varies according to APOE isotype. *Research Square Platform LLC*. 2023:rs.3.rs-2524641.
97. Farrer LA, Cupples LA, Haines JL, et al, for the APOE and Alzheimer Disease Meta Analysis Consortium. Effects of age, sex, and ethnicity on the association between Apolipoprotein E genotype and Alzheimer disease. *JAMA*. 1997;278:1349-1356.
98. Osuntokun BO, Sahota A, Ogunniyi AO, et al. Lack of an association between the E4 allele of ApoE and Alzheimer's disease in elderly Nigerians. *Ann Neurol*. 1995;38:463-465.
99. Tang MX, Maestre G, Tsai WY, et al. Relative risk of Alzheimer disease and age-at-onset distributions, based on APOE genotypes among elderly African Americans, Caucasians, and Hispanics in New York City. *Am J Hum Genet*. 1996;58:574-584.
100. Reitz C, Mayeux R. Genetics of Alzheimer's disease in Caribbean Hispanic and African American populations. *Biol Psychiatry*. 2014;75:534-541.
101. Reiman EM, Arboleda-Velasquez JF, Quiroz YT, et al. Exceptionally low likelihood of Alzheimer's dementia in APOE2 homozygotes from a 5000-person neuropathological study. *Nat Commun*. 2020;11:667.
102. Arboleda-Velasquez JF, Lopera F, O'Hare M, et al. Resistance to autosomal dominant Alzheimer's disease in an APOE3 Christchurch homozygote: a case report. *Nat Med*. 2019;25:1680-1683.
103. Mauch DH, Nägler K, Schumacher S, et al. CNS synaptogenesis promoted by glia-derived cholesterol. *Science*. 2001;294:1354-1357.
104. Kim J, Basak JM, Holtzman DM. The Role of Apolipoprotein E in Alzheimer's Disease. *Neuron*. 2009;63:287-303.
105. Lohse P, Brewer HB 3rd, Meng MS, Skarlatos SI, LaRosa JC. Familial apolipoprotein E deficiency and type III hyperlipoproteinemia due to a premature stop codon in the apolipoprotein E gene. *J Lipid Res*. 1992;33:1583-1590.
106. Mak AC, Pullinger CR, Tang LF, et al. Effects of the absence of apolipoprotein e on lipoproteins, neurocognitive function, and retinal function. *JAMA Neurol*. 2014;71:1228-1236.
107. Huang YA, Zhou B, Nabet AM, Wernig M, Südhof TC. Differential signaling mediated by ApoE2, ApoE3, and ApoE4 in human neurons parallels Alzheimer's disease risk. *J Neurosci*. 2019;39:7408-7427.
108. Weisgraber KH, Innerarity TL, Mahley RW. Abnormal lipoprotein receptor-binding activity of the human E apoprotein due to cysteine-arginine interchange at a single site. *J Biol Chem*. 1982;257:2518-2521.
109. Bu G. APOE targeting strategy in Alzheimer's disease: lessons learned from protective variants. *Mol Neurodegener*. 2022;17:51.

15525279, 2024, 4, Downloaded from https://alz-journals.onlinelibrary.wiley.com/doi/10.1002/alz.13703 by Cochrane Luxembourg, Wiley Online Library on [23/01/2026]. See the Terms and Conditions (https://onlinelibrary.wiley.com/terms-and-conditions) on Wiley Online Library for rules of use; OA articles are governed by the applicable Creative Commons License

110. Janus C, Flores AY, Xu G, Borchelt DR. Behavioral abnormalities in APPSwe/PS1dE9 mouse model of AD-like pathology: comparative analysis across multiple behavioral domains. *Neurobiol Aging*. 2015;36:2519-2532.
111. Savonenko A, Xu GM, Melnikova T, et al. Episodic-like memory deficits in the APPswe/PS1dE9 mouse model of Alzheimer's disease: relationships to beta-amyloid deposition and neurotransmitter abnormalities. *Neurobiol Dis*. 2005;18:602-617.
112. Devi L, Ohno M. Mitochondrial dysfunction and accumulation of the β-secretase-cleaved C-terminal fragment of APP in Alzheimer's disease transgenic mice. *Neurobiol Dis*. 2012;45:417-424.

SUPPORTING INFORMATION

Additional supporting information can be found online in the Supporting Information section at the end of this article.

How to cite this article: Ferguson CM, Hildebrand S, Godinho BMDC, et al. Silencing *Apoe* with divalent-siRNAs improves amyloid burden and activates immune response pathways in Alzheimer's disease. *Alzheimer's Dement*. 2024;20:2632–2652. https://doi.org/10.1002/alz.13703

15525279, 2024, 4, Downloaded from https://alz-journals.onlinelibrary.wiley.com/doi/10.1002/alz.13703 by Cochrane Luxembourg, Wiley Online Library on [23/01/2026]. See the Terms and Conditions (https://onlinelibrary.wiley.com/terms-and-conditions) on Wiley Online Library for rules of use; OA articles are governed by the applicable Creative Commons License